NASA-CR-194730

ORIGINAL PAGE IS
OF POOR QUALITY

FINAL
IN-46-CR
OCT
198175

38 P

THE UNIVERSITY OF MICHIGAN
DEPARTMENT OF ATMOSPHERIC, OCEANIC, AND SPACE SCIENCE
Space Physics Research Laboratory
2245 Hayward Street
Ann Arbor, Michigan 48109-2143

Contract/Grant Number	NAG8-919
Project Name	Multiorder Etalon Sounder (MOES) Development and Test for Balloon Experiment
Report Author(s)	Paul B. Hays
Author(s) Phone	313/764-7220
	Jinxue Wnag
	Jian Wu
Report Date	14 December 1993
Report Type	Final Technical Report
Period Covered	10 June 1992 through 31 December 1993
Project Director:	Paul B. Hays
Principal Investigator(s)	Paul B. Hays, and Jinxue Wang Space Physics Research Laboratory Department of Atmospheric, Oceanic and Space Science University of Michigan Ann Arbor, Michigan 48109-2143
Program Technical Officer	Ronald J. Koczor
Address	PS01, Building 4481 NASA MSFC Marshall Space Flight Center Alabama 35812
UM Authorization (when required)	

(NASA-CR-194730) MULTIORDER ETALON SOUNDER (MOES) DEVELOPMENT AND TEST FOR BALLOON EXPERIMENT Final Technical Report, 10 Jun. 1992 - 31 Dec. 1993 (Michigan Univ.) 38 p

N94-22026

Unclas

G3/46 0198175

ORIGINAL PAGE IS
OF POOR QUALITY

ORIGINAL CONTAINS
COLOR ILLUSTRATIONS

TABLE OF CONTENTS

ABSTRACT

The Fabry-Perot interferometer (FPI), with its high throughput and high spectral resolution has been used in the remote-sensing measurements of the earth's atmospheric composition, winds, and temperatures. The most recent satellite instruments include the Fabry-Perot interferometer flown on the Dynamics Explorer-2 (DE-2), the High Resolution Doppler Imager (HRDI), and the Cryogenic Limb Array Etalon Spectrometer (CLAES) flown on the Upper Atmosphere Research Satellite (UARS). These instruments measure the Doppler line profiles of the emission and absorption of certain atmospheric species (such as atomic oxygen) in the visible and infrared spectral region. The successful space flight of DE-FPI, HRDI and CLAES on UARS have demonstrated the extremely high spectral resolution and ruggedness of the etalon system for the remote sensing of earth and planetary atmospheres.

Recently, an innovative FPI focal plane detection technique called the Circle-to-Line Interferometer Optical (CLIO) system was invented at the Space Physics Research Laboratory. The CLIO simplifies the FPI focal plane detection process by converting the circular rings or fringes into a linear pattern similar to that produced by a conventional spectrometer, while retaining the throughput advantage of the etalon interferometer. The combination of FPI and CLIO allows the development of more sensitive Fabry-Perot interferometers in the infrared for the remote sensing of the lower atmospheres of Earth and possibly other planets. The Multiorder Etalon Sounder(MOES), a combination of the rugged etalon and the CLIO, compares very favorably to other space-borne optical instruments in terms of performance versus complexity. The new instrument is expected to be rugged, compact, and very suitable for an operational temperature and moisture sounder. With this technique, the contamination of radiance measurements by emissions of other gases is also minimized.

We at the Space Physics Research Laboratory (SPRL) have been working on the MOES concept and laboratory experiments for the past several years. Both theoretical studies and laboratory prototype experiments have shown that MOES is very competitive compared with other high resolution sounders in terms of complexity and performance and has great potential as a compact and rugged high resolution atmospheric temperature and trace species sounder from the polar platform or the geostationary platform. The logical next step is to convert our laboratory prototype to a balloon instrument, so that field test of MOES can be carried out to prove the feasibility and capability of this new technology.

This report described some of the activities related to the development of MOES for a possible balloon flight demonstration. Those research activities include the imaging quality study on the CLIO, the design and construction of a MOES laboratory prototype, the test and calibration of the MOES prototype, and the design of the balloon flight gondola.

1.0 BACKGROUND AND OBJECTIVE

1.1 Scientific Background

The launch of the Medium Resolution Infrared Radiometer (MRIR) (Norberg *et al.*, 1966) on TIROS-7 in 1966 established the value of atmospheric temperature profiling by measuring the upwelling thermal radiance in the 15 μm band of carbon dioxide (CO_2) with satellite instruments. Since MRIR, considerable progress has been made in the development of more advanced satellite instruments for the passive infrared remote sensing of atmosphere temperature profiles. However, most of those sounders are low spectral resolution instruments, leading to broad weighting functions and low vertical resolution. The development of supercomputers make it possible to model the atmosphere with ever increasing spatial and spectral resolution, there is urgent need for more accurate soundings of the atmospheric temperature and moisture profiles to serve the needs of numerical forecasting, atmospheric chemistry and global ozone studies, and global change research. But up to now, those requirements have not been met by the current operational meteorological sounders, such as the HIRS/2, mainly due to their low spectral resolution.

Clearly the current generation of sensors to measure the atmospheric constituents and temperature profiles need to be improved to meet the future requirements of atmospheric science community. Associated with this desire for improved instrumentation is a strong need to develop high resolution atmospheric sensors with reduced cost and complexity. Theoretically, the temperature profile of the atmosphere can be derived from either the CO_2 band structure or the structure of the pressure/Doppler broadened CO_2 lines. All the previous temperature sounders used CO_2 band structure to derive the atmospheric temperature profile because of limitations by signal to noise and spectral resolution. But with the development of more sensitive detectors and the use of advanced high resolution interferometers, such as the Michelson interferometer or Fabry-Perot interferometer, it becomes feasible to derive atmospheric temperature profiles from the structures of the CO_2 spectral lines. This approach has similarities to the selection of sounding channels for the microwave sounders (such as MSU or AMSU). In the design of the microwave sounders, no attempt has been made to survey large regions of the O_2 band, rather efforts have been directed at measuring portions of a single O_2 spectral line with high resolution and accuracy.

It is well known that the limitation in vertical resolution is caused mainly by the broadness of the weighting functions of the current instruments which is largely due to their low spectral resolution. When the weighting functions are broad, emitted energy reaching the sounder in each channel has components originating from a thick layer of the atmosphere, making the retrieval of the fine scale vertical structures practically impossible. One way to decrease the width of the weighting functions and improve the vertical resolution and accuracy of remote temperature sounding is to use instruments of higher spectral resolution, which are able to resolve the individual spectral lines. High spectral resolution with limited integration time posed by satellite operation results in low signal, and low signal to noise will reduce the accuracy of the temperature sounding. So the question is how can we have both high spectral resolution and good signal to noise? It has been known for a long time that CO_2 has a periodic spectrum in its P and R branches of the 15 μm and 4.3 μm bands (Houghton, 1961). FPI is a periodic high resolution and high throughput instrument, which makes it an ideal instrument to observe the periodic CO_2 spectrum. By matching the period of the FPI with the spacing of CO_2 spectral lines and observing a series of spectral lines simultaneously with a multiorder FPI, high spectral resolution can be achieved with a relatively high signal level. Recently, researchers at the Space Physics Research Laboratory (SPRL) of the University of Michigan developed a new FPI focal plane detection technique and device, the circle to line converter (Hays, 1990). This device can be used with a conventional FPI to convert the circular interferometric pattern into a linear pattern that can be used with linear array detectors. The Multiorder Etalon Sounder (MOES), a combination of FPI and the circle to line converter, compares very favorably to other space-borne optical instruments in terms of performance versus complexity. The new instrument is expected to be rugged, compact, and very suitable for an operational temperature and moisture

sounder. With this technique, the contamination of radiance measurements by emissions of other gases is also minimized. Because of its ruggedness and the fact that no complicated mechanical spectral scanning scheme is needed, MOES is also very attractive for planetary exploration.

We at SPRL together with scientists and engineers from ITT Aerospace Communications Division (ITT-ACD) have done some preliminary studies on the feasibility of MOES as a next-generation high resolution infrared sounder of the earth's atmosphere on NOAA meteorological satellites (Wang *et al.*, 1993; Wang, 1990). Performance simulation studies of MOES by using the Minimum Variance Simultaneous (MVS) retrieval method developed at the National Environmental Satellite Data and Information Services of NOAA (NOAA/NESDIS) (Fleming *et al.*, 1986) indicate that MOES can provide more accurate temperature and water vapor profiles than that provided by the current operational infrared sounder HIRS/2 (Fleming, private communication, 1990). As an example, the simulation results of MOES as a high resolution infrared sounder of the earth's atmosphere for January 60° to 30° North is shown in Fig. 1.1. The improvement in temperature and moisture retrieval accuracy is mainly due to the much higher spectral resolution of MOES and its ability to resolve a single CO_2 spectral line.

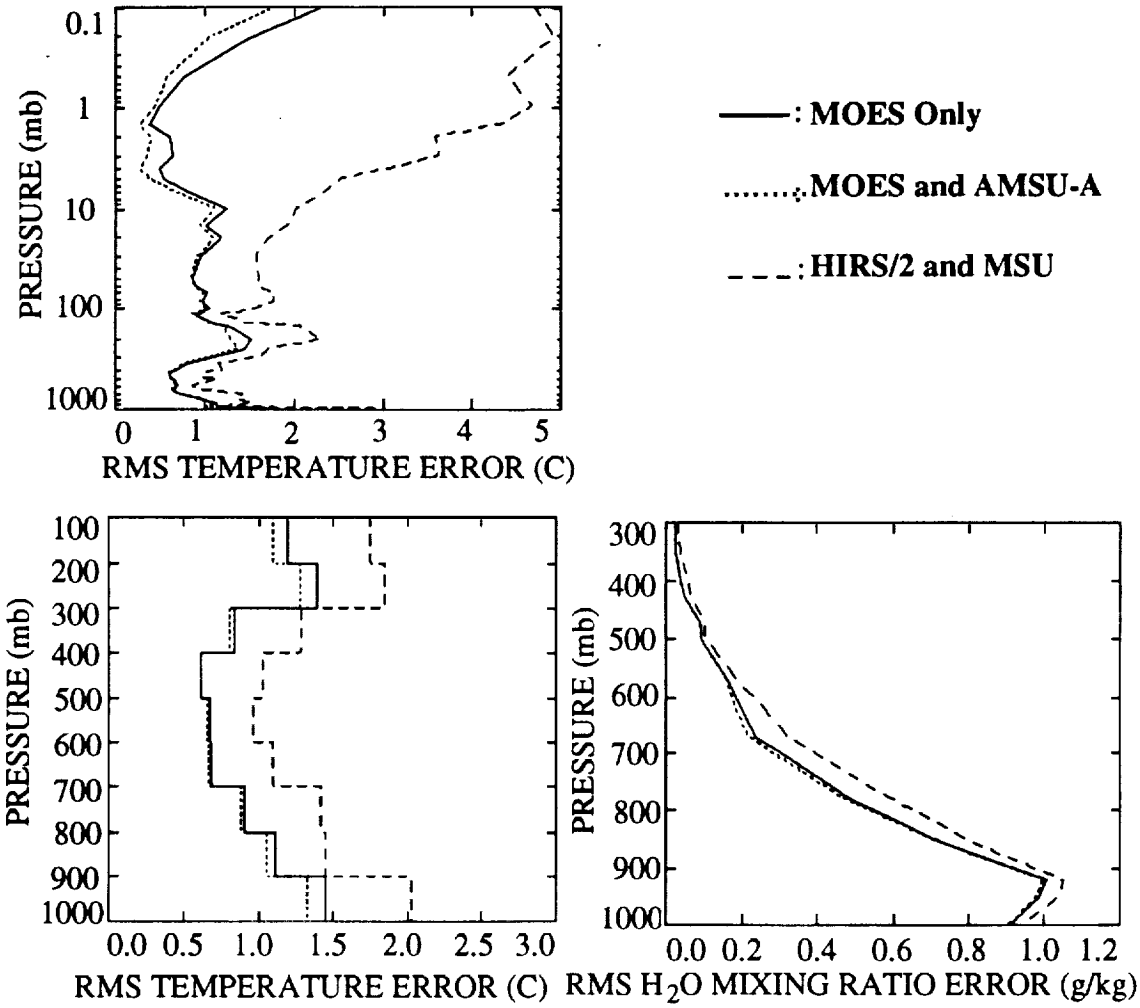

Fig. 1.1. RMS temperature and moisture errors of MOES only, MOES and AMSU-A, HIRS/2 and MSU generated by the MVS retrieval algorithm for January 60° to 30° North.

1.2 Objectives

The main objective of the MOES development and test for balloon experiment project is to carry out important design and laboratory study of MOES to ensure a quick implementation of a balloon flight demonstration if the opportunity arises. The following tasks were carried out to support this objective:

(1) Evaluation of the CLIO imaging quality and design tolerance, CLIO is a critical new FPI detection technology in MOES.

(2) The design and construction of a laboratory prototype MOES to identify possible technical problems and gain experience for possible future balloon-based or satellite-born MOES development.

(3) Test and calibration of the laboratory prototype. Channel registration and spectral resolution measurements.

(4) Design of balloon-flight gondola and determination of weight and size requirements.

2.0 CLIO IMAGING QUALITY STUDY

2.1 Theory of the Circle to Line Interferometer Optical (CLIO) System

The Fabry-Perot interferometer creates a series of rings at the focal plane of the system, special detectors and scanning strategies are needed to analyze the circular interference fringes and to extract useful spectral information. The Circle to Line Interferometer Optical (CLIO) system will convert the circular rings or fringes into a linear pattern similar to that produced by a conventional spectrometer, while retaining the basic throughput advantage of the Fabry-Perot interferometer. The resulting linear fringe pattern can be measured by using commercially available CCD detectors or linear array detectors. By placing a 45 degree cone at the focal plane, the series of rings are converted into a series of spots on the optical axis. But the cone projects only one quarter of the ring effectively onto a detector element, while three fourth of the signal is lost. This problem is solved by using a mirrored kaleidoscope which consists of two mirrors joined at the optical axis of the lens system and terminated by the cone. The function of the kaleidoscope is to transform an entire circular ring into a ring segment which is subsequently focused onto a detector element by the cone. The complete circle to line interferometer optical system is shown in Fig. 2.1. The combination of CLIO and high quantum efficiency solid state detectors makes the Fabry-Perot interferometer more sensitive for aeronomy and atmospheric remote sensing applications.

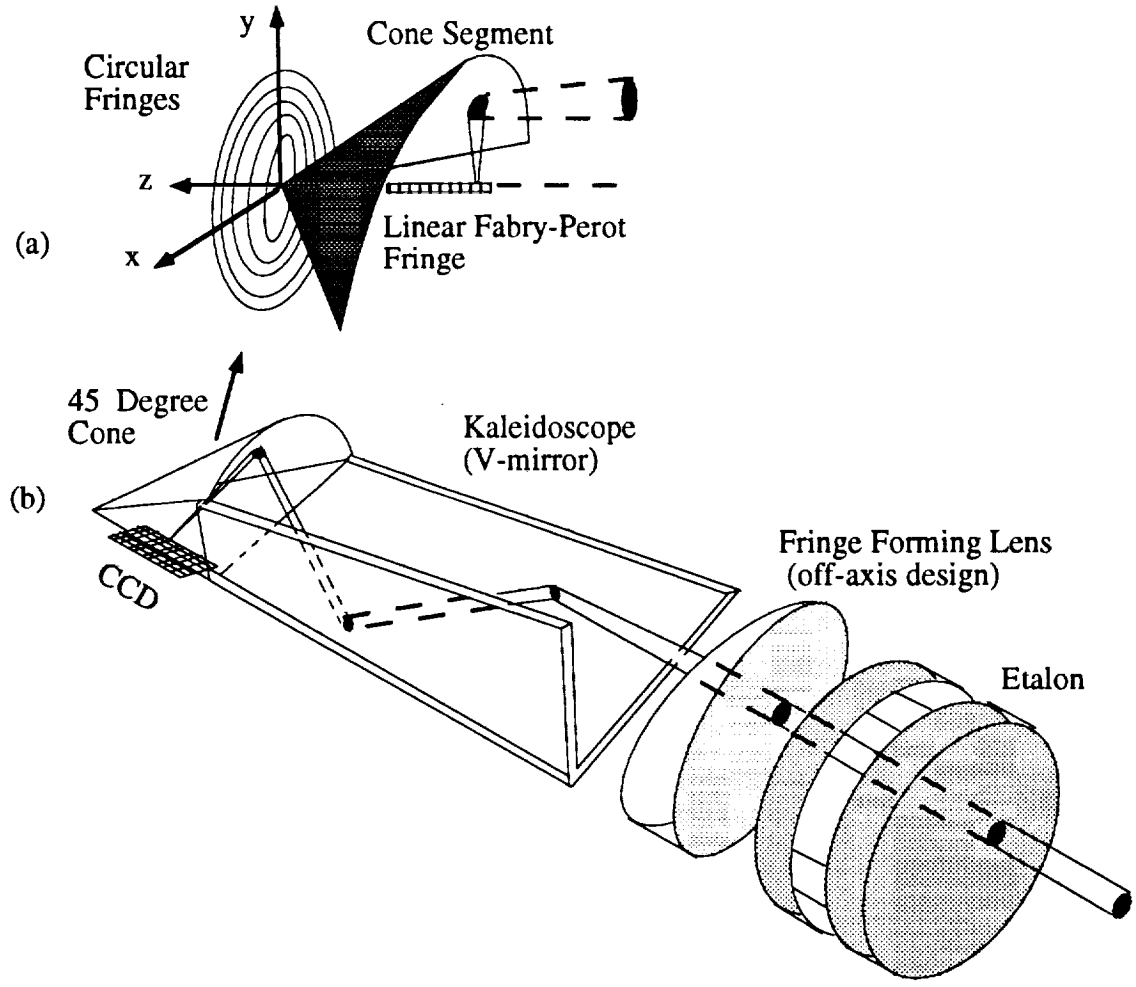

Fig. 2.1. (a) Illustration of the conversion of a ring segment into a spot by the cone.
(b) Schematic diagram of the circle to line interferometer optical system.

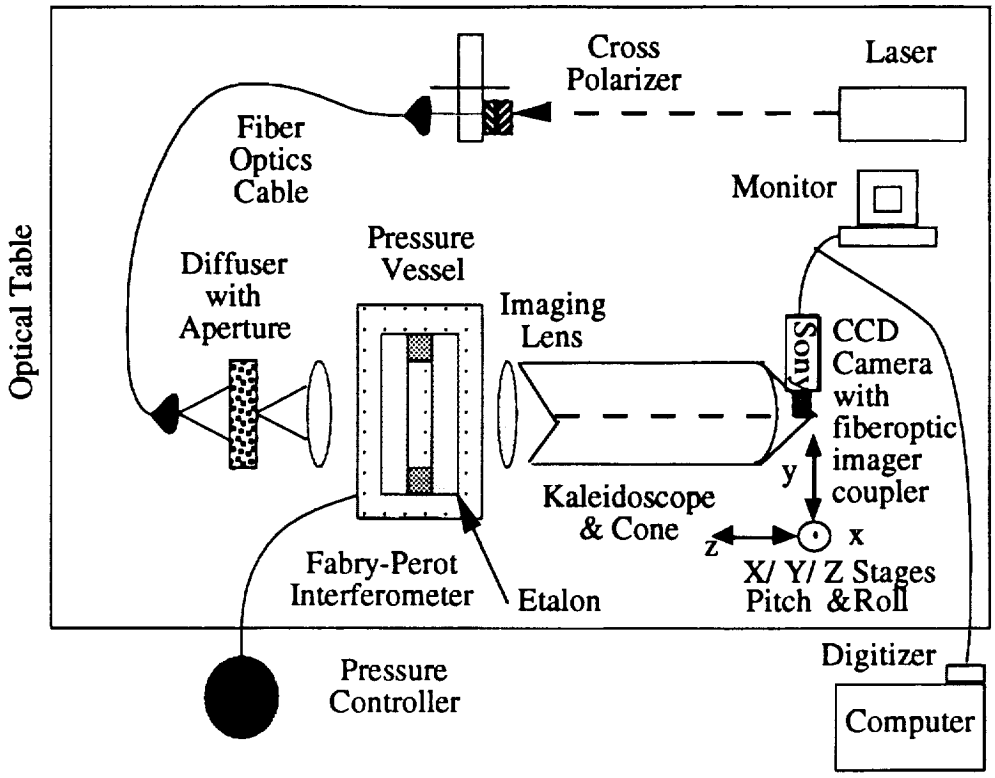

Fig. 2.2. CLIO imaging quality and tolerance study set-up.

2.2 Laboratory CLIO Imaging Quality Study Set-up

The schematic diagram of the laboratory study set-up is shown in Fig. 2.2. A Spectra-Physics single mode He-Ne laser served as the source. The laser light was introduced to the FPI light expansion and collimation optics through a fiber optics cable. A ground glass diffuser, an aperture, and lenses were used to expand, diffuse, and collimate the laser light beam into the etalon. Those elements were carefully aligned so as to get a uniform illumination. The Fabry-Perot etalon plates were made of fused silica with high reflectivity coating on the inner surfaces. The gap between the two etalon plates is 7 mm. The etalon was housed in a chamber. The pressure inside the chamber can be changed by a pressure stepper for some fine adjustment of the FPI transmission function. A 45° half angle internally reflecting cone manufactured by single-point diamond turning was mounted on a three-dimensional translation and two-axis rotation stage. The rotation about z axis is not important and therefore was not included in the degrees of motion. The cone axis is designed to be coincident with the main optical axis that is perpendicular to the etalon surfaces. The position of cone apex should be on the focal plane of the objective lens. A v-shape mirror composed of two plane mirrors perpendicular to each other forms the kaleidoscope, which was mounted on a two-dimensional translation (x and y) and three-axis rotation stage. The translation motion along z axis does not affect the performance of CLIO, so this translation was not included in the set-up. Another degree of freedom was the angle between the two mirrors. For this experiment, the kaleidoscope axis, the optical axis of the objective lens, and the cone axis need to be on the main optical axis of the FPI system. Initially a Pulnix camera with a camera lens was used, because the CCD chip can not be placed at the focal plane, we had to take the images of the fringes on a screen placed at the focal plane, this process caused some degradation to the sharpness of the fringes. In order to solve this problem, we used a model iS 558 CCD camera (i2S, Inc., Norwood, MA) without the camera lens, the advantage of this CCD camera is that the CCD chip can be taken out of the camera body, we modified the camera with a new front plate so that the CCD extends about 0.25" out of the camera body. With

this modified iS 558 CCD camera, the focal plane is directly accessible by the CCD chip, no re-imaging is needed. The disadvantage of the iS 558 CCD camera is that no thermoelectric cooling is available, so CCD dark count is high. In order to reduce the dark counts, we bought a Sony XC-77 CCD camera with thermoelectric cooling and a special fiber optic image coupler, the function of the image coupler is to introduce the system focal plane to the CCD chip inside the camera body. The schematic diagram of the Sony XC-77 CCD camera with fiber optic image coupler is shown in Fig. 2.3. The output signal of the CCD camera goes to a TV monitor as well as a frame grabber on a Digital workstation. Images were digitized, stored, displayed, and processed with the workstation.

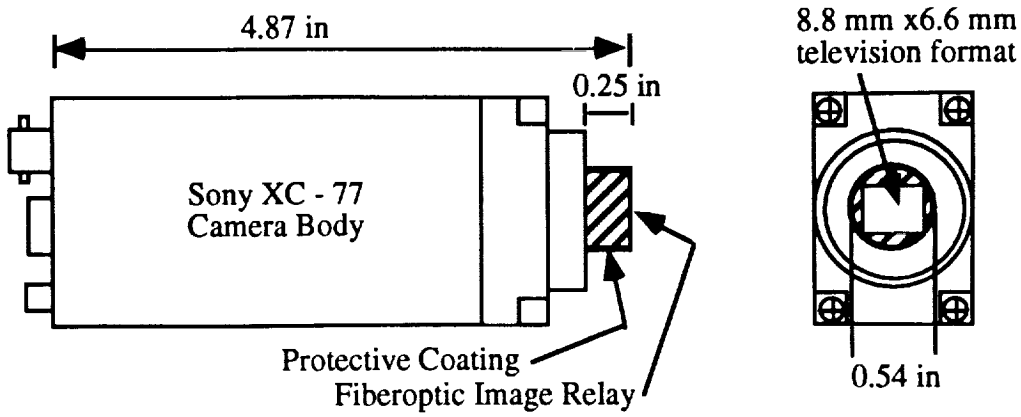

Fig. 2.3. Schematic diagram of the CCD camera with fiber optic image coupler used in CLIO imaging quality and tolerance study.

2.3 Laboratory Study Results and Discussions

The experiment procedures and results of the laboratory CLIO performance study are presented in this section. The main objective of this experiment is to study the possible image and FPI finesse degradation caused by this circle to line conversion. The image degradation is mainly caused by the broadening of the converted linear fringes along the cone axis (the image plane of this system), which leads to the degradation of the finesse of Fabry-Perot interferometer. As shown in Fig. 2.2, a stable He-Ne laser beam is coupled to the FPI collimating Optics by a optical fiber cable. The expanded and collimated laser light passes through the Fabry-Perot etalon, a concentric fringe pattern is formed at the focal plane of the imaging lens. During the experiment, we first recorded the circular fringe formed by the FPI without the kaleidoscope and cone, the image is then digitized with the frame grabber and stored in computer for processing. Then the 45° cone is placed at the system focal plane, by adjusting the orientation and position of the cone, a sharp linear fringe pattern can be observed on the monitor, the linear fringe is recorded and digitized. After the cone is properly adjusted, the kaleidoscope is placed into the system. In order to fold the whole circular fringe pattern into a 90 degree segment, the kaleidoscope needs to be carefully adjusted. If the cone and the kaleidoscope are properly adjusted, a linear fringe pattern will be observed on the monitor. The linear fringe patterns with cone and kaleidoscope is also digitized and stored in computer fro processing. Figure 2.4 is the circular fringe pattern formed by the Fabry-Perot interferometer without the CLIO, the binned one dimensional profile is shown in Fig. 2.5, the finesse of the FPI system without CLIO is 14.0. Figure 2.6 is the linear fringe pattern resulted from the conversion of one quarter of the circular fringe pattern by the 45 degree cone, the corresponding binned one dimensional profile is shown in Fig. 2.7, the finesse of the FPI with cone only is 13.5, the cone introduces very little finesse degradation. Figure 2.8 and Fig. 2.9 show the linear fringe pattern and binned one dimensional profile resulted from the conversion of the whole circular fringe pattern by both the 45 degree cone and the kaleidoscope, the finesse of the resulted linear fringe pattern is 9.6. The degradation of FPI finesse with the kaleidoscope is mainly due to the poor quality of the

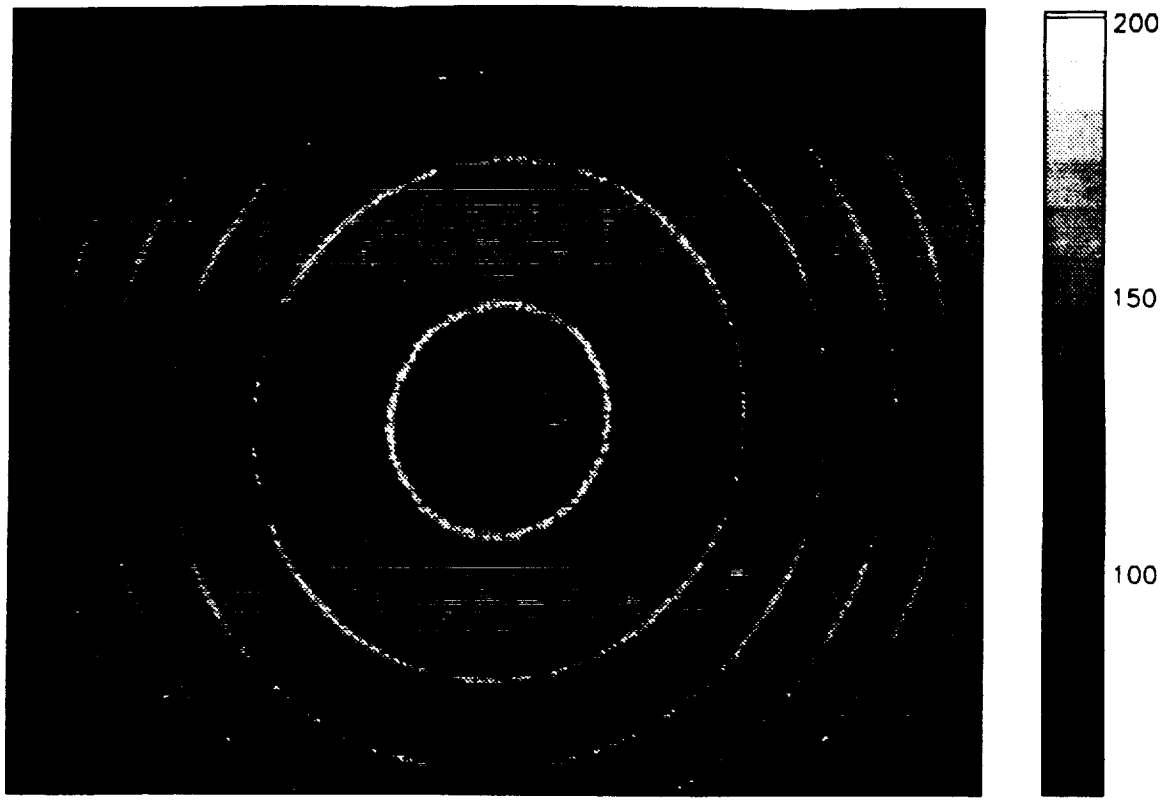

Fig. 2.4. Circular fringe pattern formed by Fabry-Perot interferometer without CLIO.

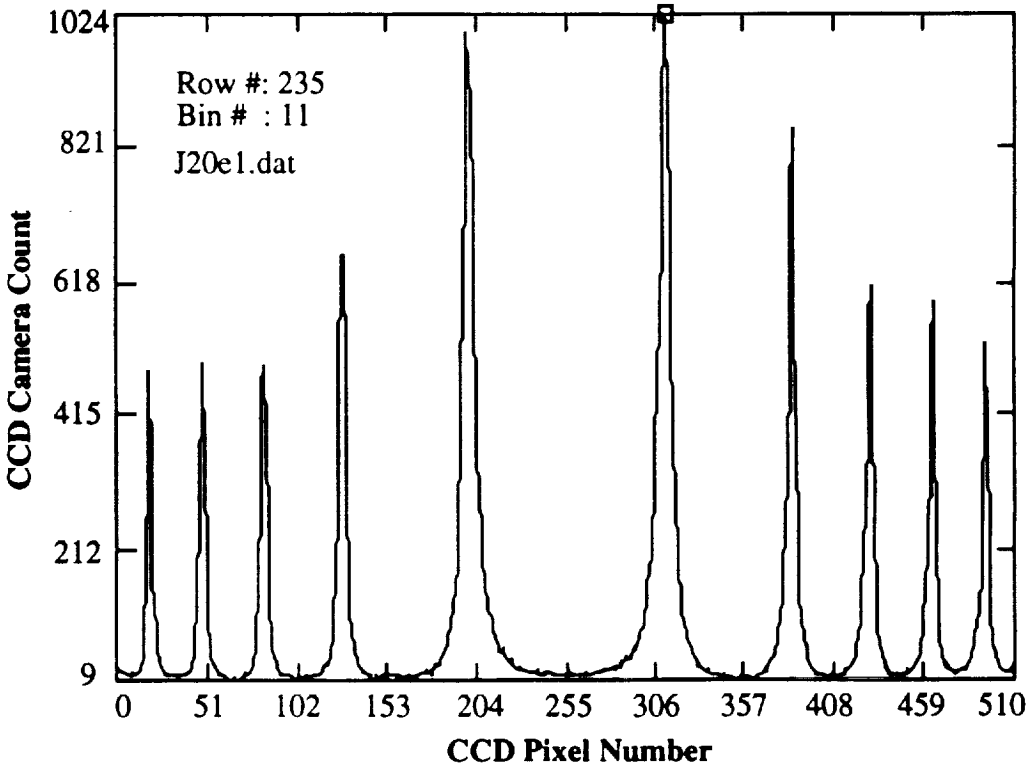

Fig. 2.5. Cross section of Fabry-Perot fringe pattern shown in Fig. 2.4, and the finesse is 14.

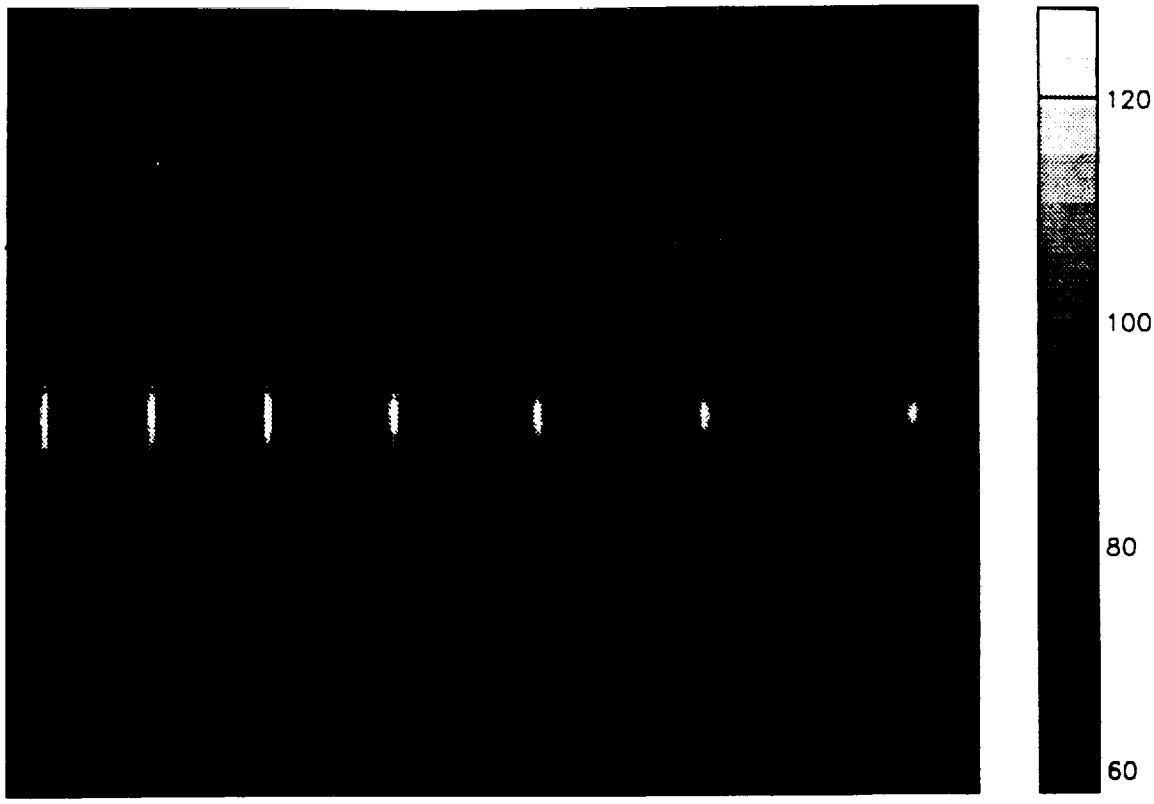

Fig. 2.6. Linear fringe pattern resulted from the conversion of one quarter of the fringe pattern by the 45 degree cone.

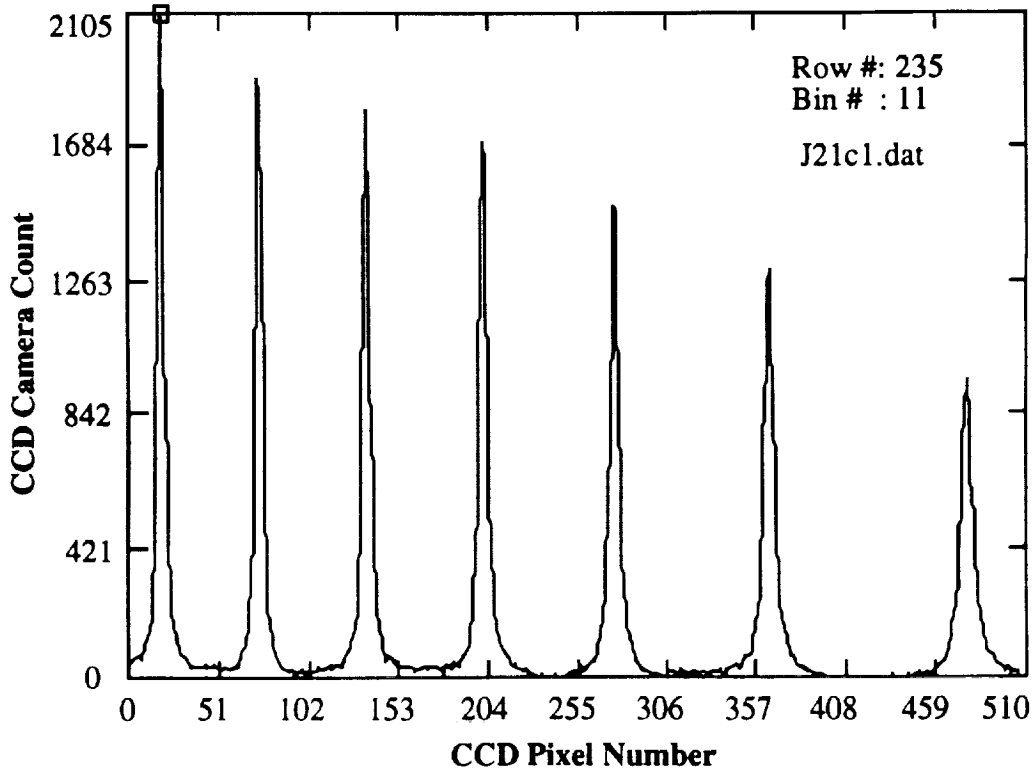

Fig. 2.7. Binned cross section of the linear fringe resulted from circle to line conversion by the 90 degree cone segment.

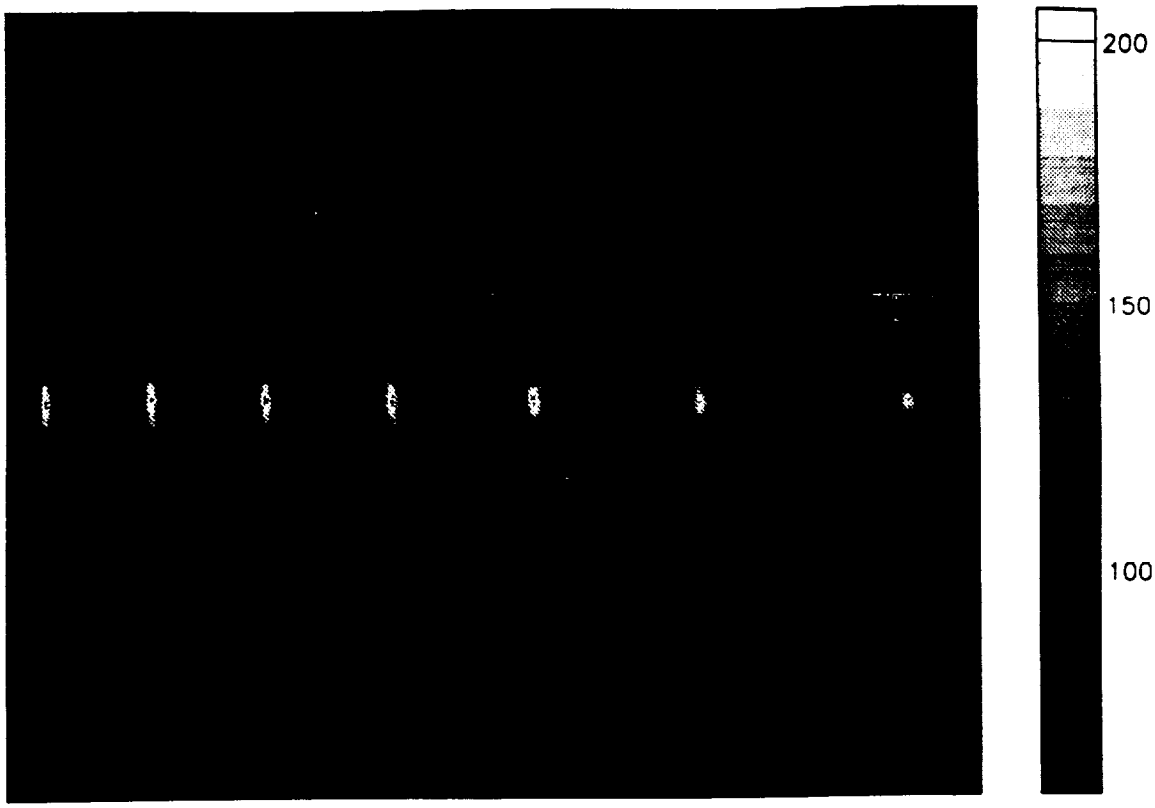

Fig. 2.8. Linear fringe pattern resulted from the conversion of the whole circular fringe by both the 45 degree cone and the kaleidoscope.

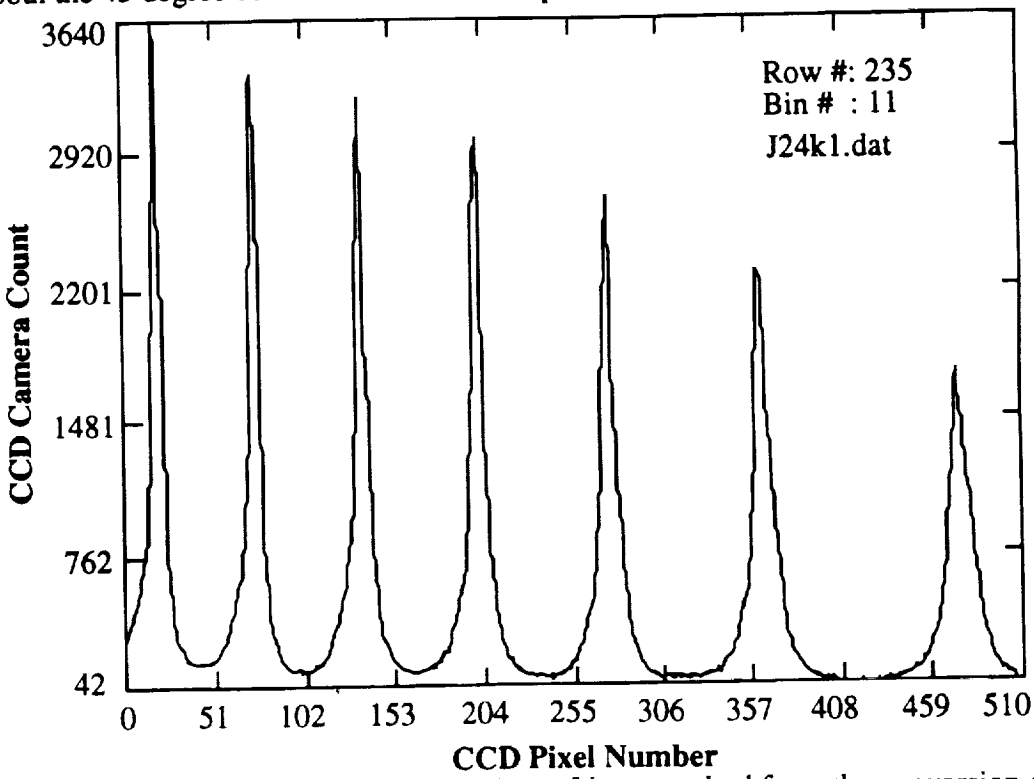

Fig. 2.9. Binned cross section of the linear fringe resulted from the conversion of a complete circular fringe pattern by the cone and kaleidoscope.

kaleidoscope mirror, which are low price glass mirrors from Edmon Scientific. Much better mirrors will be used in the CLIO of FPI systems for aeronomy and remote sensing. Compared the results here with the ray trace results in the original CLIO publication by Hays (Hays, 1990), the shapes of the linear fringes observed in the laboratory are similar to those predicted by the ray trace study. We note here that in the ray trace results the line segment seems narrower at the center than at the ends, while in the experiment results the center of the line segment is a little wider than the endpoints. This can be explained by the fact that the ray trace results were based on the conversion of a circle formed by pencil beams (each ray bundle was focused into one point forming an infinite narrow circle), while the linear fringes in the experiment were resulted from the conversion of real Fabry-Perot circular fringes of finite width with a finesse of 14. Another reason for this image difference is that the cone is not perfectly flat for He-Ne laser wavelength and causes some scattering.

For the design tolerance study, the behavior of the CLIO is investigated under misalignment conditions. Both ray trace simulation and laboratory study show some of the misalignments affect the image quality more than others. Our laboratory study show that the most critical alignment is the alignment of the kaleidoscope axis with the system optical axis. If the axis of the kaleidoscope is parallel to but not coincident with the main optical axis, the four quadrant of the line segment will separate as shown in Fig. 2.10. These four quadrant are from: light not reflected by V-mirror, light reflected by mirror 1, light reflected by mirror 2, and finally light reflected by both mirrors. When the axis of kaleidoscope is coincident with the main optical axis, these four quadrants will coincide with each other and form a narrow line segment as shown in Fig. 2.10. Our laboratory alignment tolerance study shows that CLIO is a very tolerant system, which is important for its application to space-borne FPI.

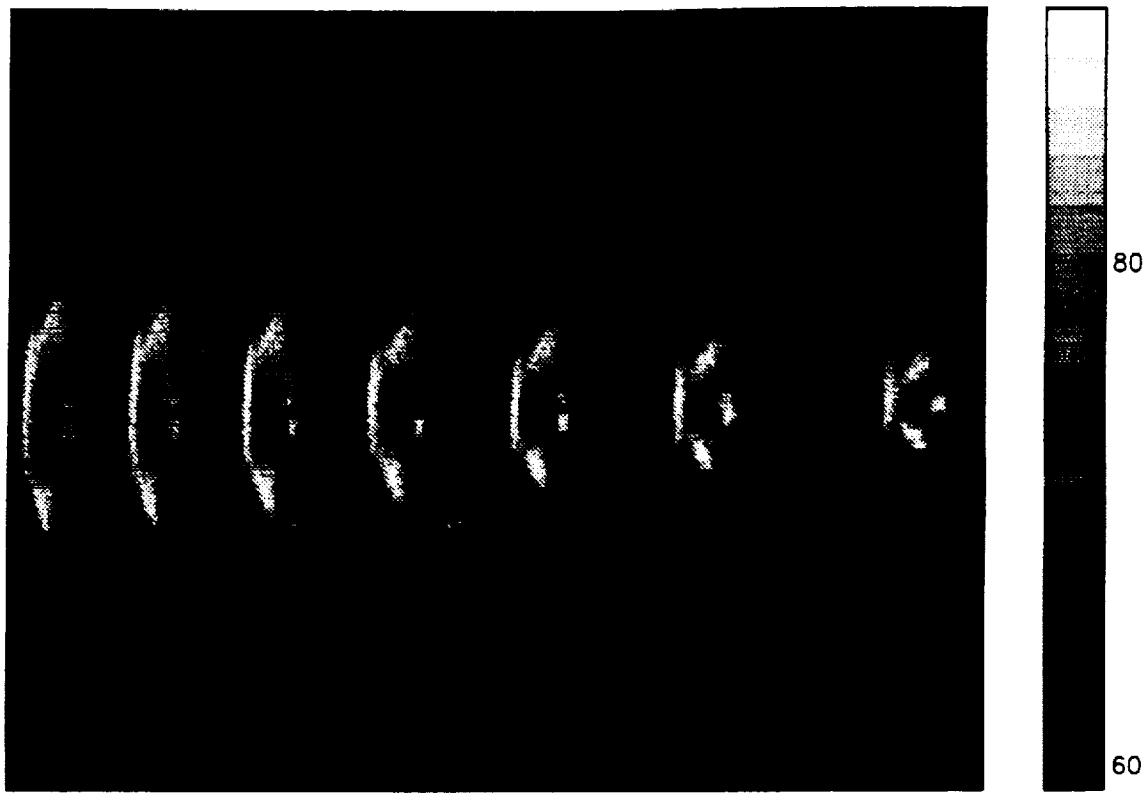

Fig. 2.10. Fringe pattern when the kaleidoscope was intentionally misaligned (translated along y axis). Note that the four quadrants are separated.

3.0 MOES LABORATORY PROTOTYPE FOR BALLOON EXPERIMENT

3.1 overall Optical and Mechanical Design

Major MOES optical subsystems will be placed in a specially designed LN2 dewar to reduce the background and increase the system sensitivity. The schematic diagram of MOES in LN2 dewar is shown in Fig. 3.1. A picture of the MOES dewar and assembly is shown in Fig. 3.2. The MOES assembly consists of a narrow band blocking filter, etalon, fringe forming lens, kaleidoscope, cone, and a linear array MCT detector. Pictures of the filter-etalon-lens-kaleidoscope-cone assembly for MOES tropospheric temperature sounding are shown in Fig. 3.3. The design and characteristics of each components are described in the following sections.

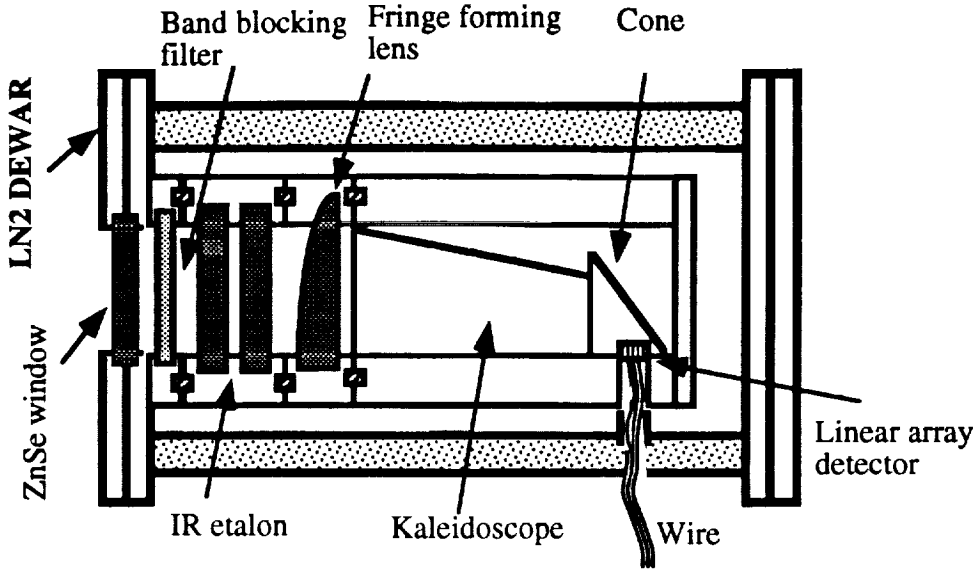

Fig. 3.1. Schematic diagram of MOES tropospheric temperature sounding band in LN2 dewar.

3.2 Band Blocking Filter

The band blocking filter is to isolate the CO_2 band from 725.0 cm^{-1} - 747.0 cm^{-1}. It is manufactured by the Optical Coating Laboratory, Inc. (OCLI). Its characteristics is listed below.

Substrate material:	Ge
Operating temperature:	80 K
Center wavelength λ_0:	13.582 μm
Half bandwidth:	0.3232 μm
Peak transmission:	79%
Blocking:	</= 0.1% average below and above band to 17 μm
Diameter:	38.10 μm
Clear aperture:	34.00 μm

One issue in the design of the filter is the substrate material. Because ZnSe transmits He-Ne laser light at 6328.0 Å, which makes instrument alignment easier by using a He-Ne laser. We could arrange to have a small area on the ZnSe filter substrate uncoated to facilitate alignment by using a He-Ne laser, but this will drive up the cost of the filter too much for our MOES laboratory prototype project.

ORIGINAL PAGE
COLOR PHOTOGRAPH

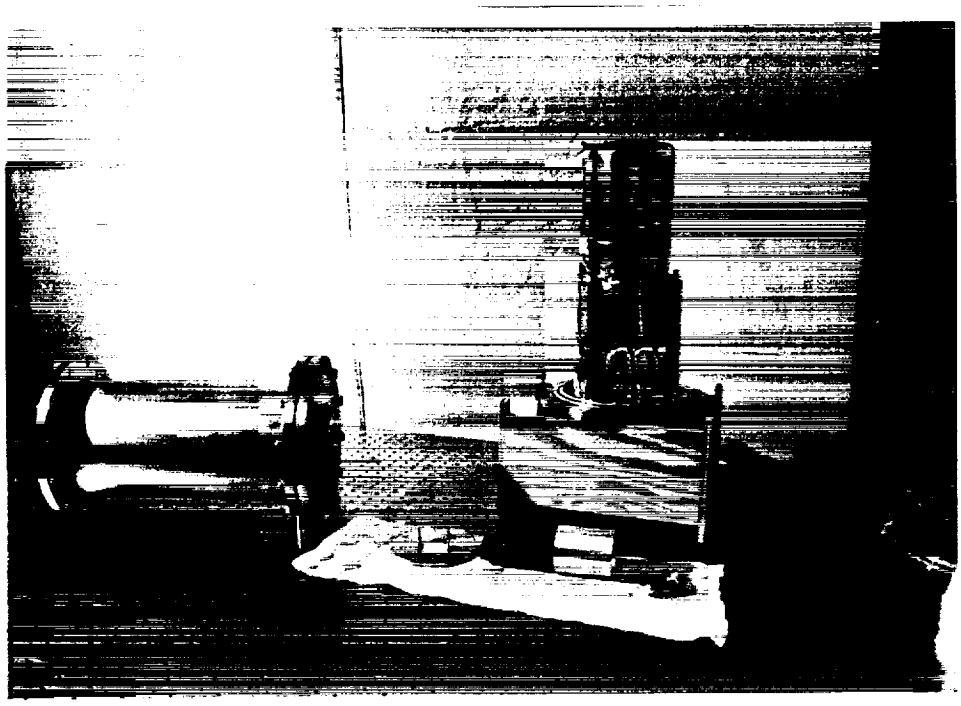

Fig. 3.2. Picture of the MOES laboratory prototype LN2 dewar and assembly.

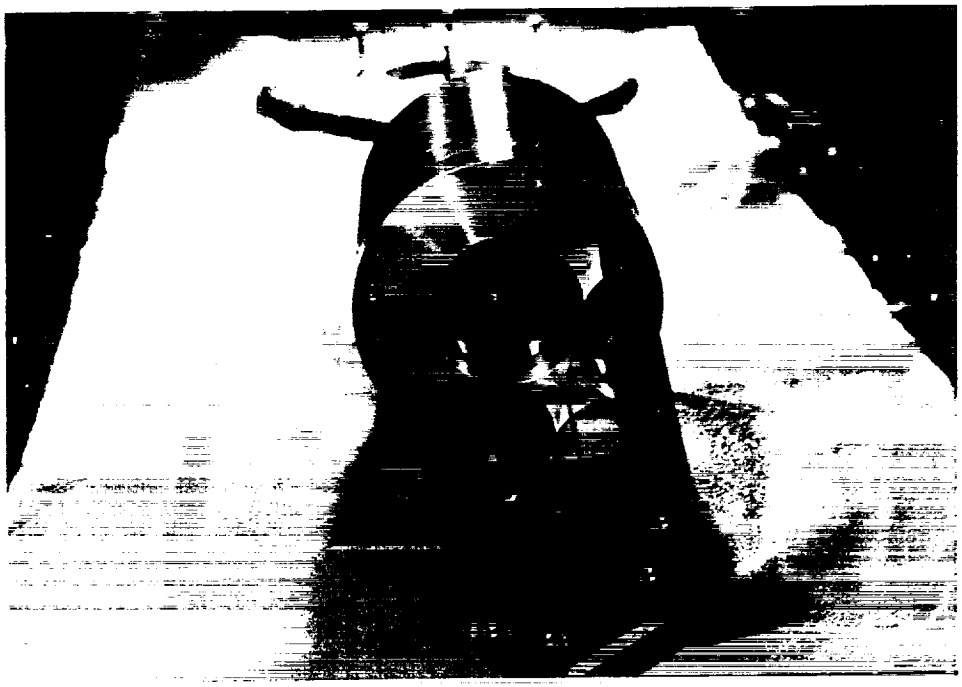

Fig. 3.3. Picture of the filter-etalon-lens-kaleidoscope-cone assembly for the single band MOES laboratory prototype.

3.3 Etalon and Etalon Holder Design

The Fabry-Perot etalon is the key component of MOES. Several options, the fixed air gap etalon, the solid etalon, or a piezo-electrically controlled etalon have been examined in the design process. We have also consulted with several manufactures in order to come up with the best design with the least cost. The advantages, disadvantages, and the state-of-the-art technologies in producing those etalons are described below.

Solid etalon is potentially a easy and cost effective approach, but the free spectral range requirements of some of the MOES etalons result in very thin solid etalons. For example, the optimum free spectral range for the MOES tropospheric temperature sounding band etalon is 1.53 cm^{-1}. With a ZnSe refractive index of 2.40, the thickness of the solid etalon is d = 1/(2x1.53x2.4) = 0.136 cm = 1.36 mm. This is not impossible, Perkin Elmer (now called the Hughes Danbury Optical Systems, Inc.) has produced even thinner etalons. One has to be very careful in dealing with those very thin etalons and special holders are needed. Another disadvantage of the solid etalons is that the etalon gap can not be adjusted. Since in our application, certain adjustments of the etalon gaps are needed to get the correct gap thickness and channel positions, especially in the laboratory calibration stage, we decided not to use solid etalons.

Piezo-electrically tuned etalon in the IR are available from Queensgate Instruments Ltd. The etalons can be cooled to cryogenic temperature and servo-stabilized to achieve high levels of stability. Piezo-electric actuators cemented between the mirrors make the etalon tunable by up to 15 orders of interference about a nominally fixed cavity length. Etalons with clear apertures from 28 mm to 140 mm are available fabricated in ZnSe for 3 - 15 μm applications. The etalons are cell mounted with flying leads for ease of mechanical and electrical installation. This new piezo-electrically tuned etalon for low temperature operation is potentially a very good option for our purpose. Unfortunately, it is expensive and out of our budget for the laboratory prototype.

Fixed air gap etalon is a reasonably mature technology, SPRL has a lot of experience in working with fixed air gap etalon, the etalons used in both the Dynamics Explorer (DE) FPI and the High Resolution Doppler Imager (HRDI) on the Upper Atmospheric Research Satellite (UARS) are fixed air gap etalons. The etalons for DE-FPI and HRDI are for the visible, the etalon plates are made of fused silica, and the spacer posts and the plates can be optically contacted. The etalons in MOES are for the infrared, the appropriate etalon plates material is ZnSe. The properties of ZnSe make it impossible to optically contact the plates and the spacer posts. In order to produce a fixed air gap etalon with ZnSe, other methods of holding the plates and posts together are needed. We could use super glue to put them together, but once they are glued together, it is very hard to take them apart without destroying the plates. Since it might take several iterations to get the correct etalon, this approach may greatly increase the cost of the project. Another more promising approach is to make a special etalon holder to hold the etalon plates together. We have designed and manufactured an etalon holder at SPRL similar to that used in the DE-FPI. This Hasen mount features thermal isolation of the etalon plates from the chamber. Three springs, mounted and designed to minimize mechanical vibration as well as thermal variability, evenly distribute force upon three ZnSe spacers that establish the etalon's gap. Force on the plates where these springs contact is adjusted by a geared thumbwheel assembly to optimize parallelism and minimize distortions between the etalon plates. The etalon plates and spacers for MOES prototype are manufactured by II-VI incorporated. The inner surfaces of the etalon are matched to $\lambda/120$, the back surfaces are plane to $\lambda/20$ and wedged at 49 arc minutes to cast multiple reflections out of the instrument optical path. The coating are done at λ_0 = 13.6 μm, a reflectivity of 93.5% for both plates are achieved. Measurements of the assembled etalon in the laboratory show that a finesse of 33 and peak transmission of 72.5% have been achieved. A picture of etalon in the holder is shown in Fig. 3.4, the three springs can be seen clearly.

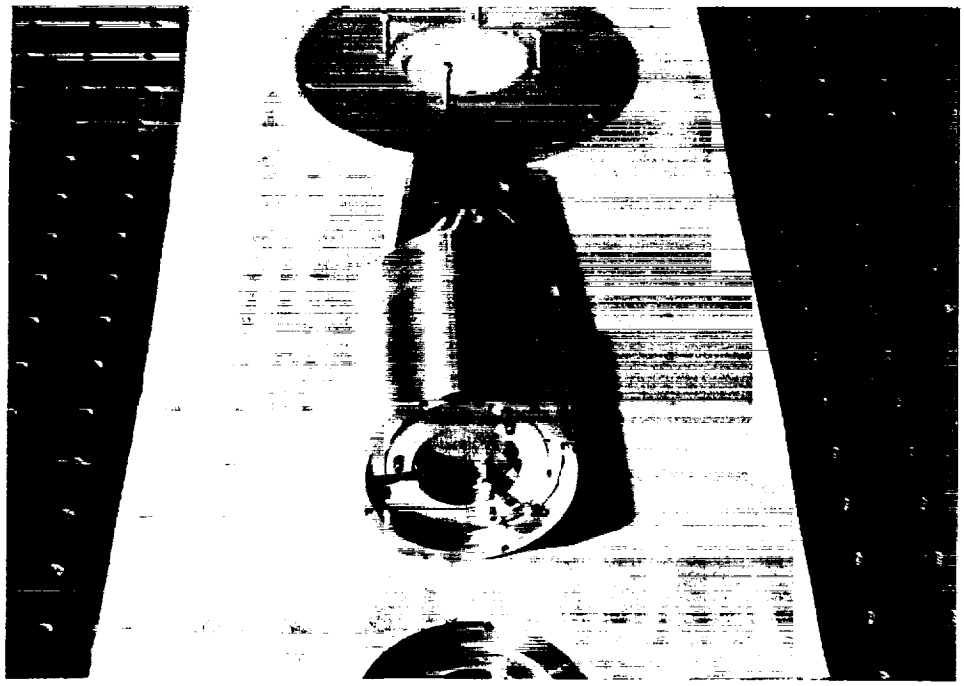

Fig. 3.4. Picture of the etalon in the specially designed DE-FPI type holder.

3.4 Fringe Forming Lens Design

The design of the fringe forming lens has gone through several modifications mainly because the difficulty of finding a supplier. The lens used in MOES is not a conventional lens, we need a whole lens that functions like one quarter of a lens. We could use only one quarter of a very large lens, but this approach will increase the size and weight of the system. The initial design called for a quarter of a doublet, then it was thought that a single aspheric lens might give better imaging quality, so a quarter of a single aspheric lens design was adopted. II-VI incorporated initially suggested that they can manufacture the lens for us by first producing a single aspheric lens and then cut it. But after more careful examination of the process, II-VI told us that they can not produce the lens as suggested before. Laser Power Optics suggested that they can provide the fringe forming lens by producing the lens as an off-axis meniscus. The off-axis design works very well and met our requirements.

3.5 Kaleidoscope and Cone Assembly Design

Considerable amount of time and efforts have been spent on the design of the kaleidoscope and cone assembly. Because it is a new device, no body has any previous experience with it. First, a laboratory design tolerance study was undertaken. The purpose of the laboratory design tolerance study is to demonstrate the overlapping of the four segments of the FPI interference fringes, the conversion of one quarter of the circular fringe into a narrow line segment as predicated by theory and ray trace, and the mechanical and optical tolerance on the kaleidoscope and cone design. With the design tolerance information from the laboratory study, we consulted with several possible metal optics suppliers with precision diamond machining facility and capability. Because of the alignment and imaging quality requirements, very high accuracy are needed in the manufacturing of the kaleidoscope and cone. The final kaleidoscope and cone assembly was manufactured by Speedring Systems by single point diamond turning of aluminum. A figure accuracy of about $\lambda/5$ at 632.8 nm and surface finish better than 100 Å have been achieved. The inner surface of the kaleidoscope and cone are gold coated by Dayton

Vacuum. The whole assembly is rugged and meets our requirements. A picture of the kaleidoscope and cone assembly is shown in Fig. 3.5.

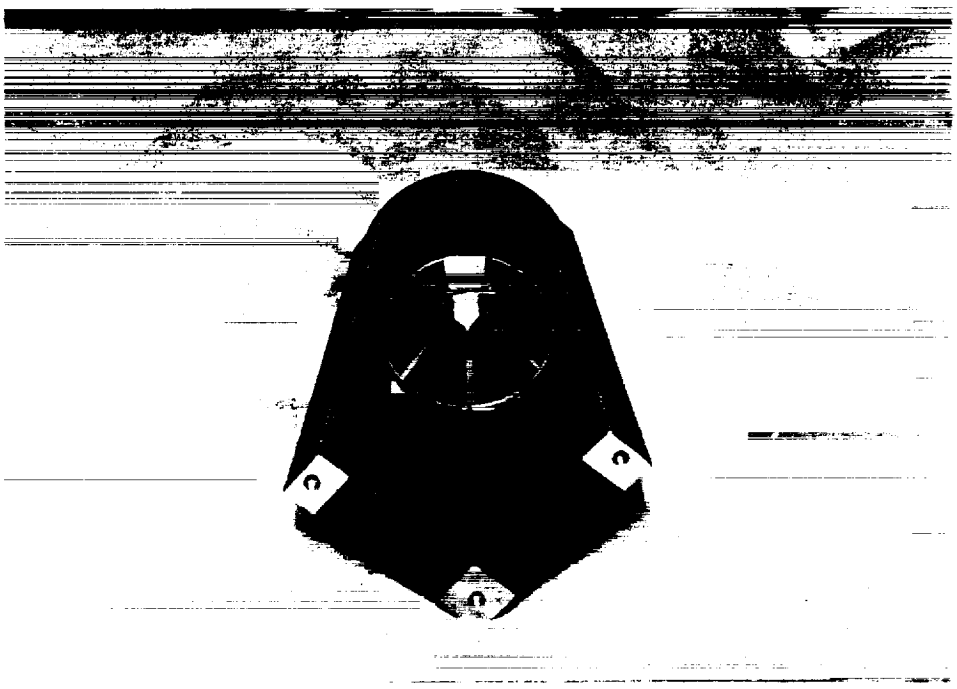

Fig. 3.5. Picture of the kaleidoscope and cone assembly manufactured by precision single point diamond turning. A figure accuracy of $\lambda/5$ at 632.8 nm and surface finish better than 100 Å have been achieved.

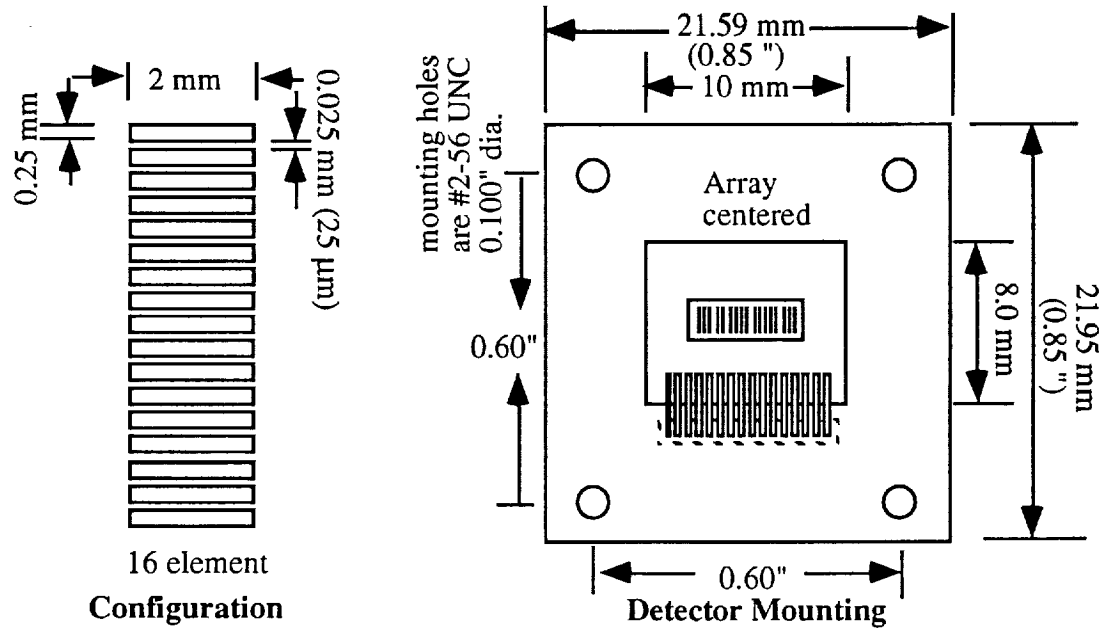

Fig. 3.6. Schematic diagram of the 16 elements MCT array for prototype MOES.

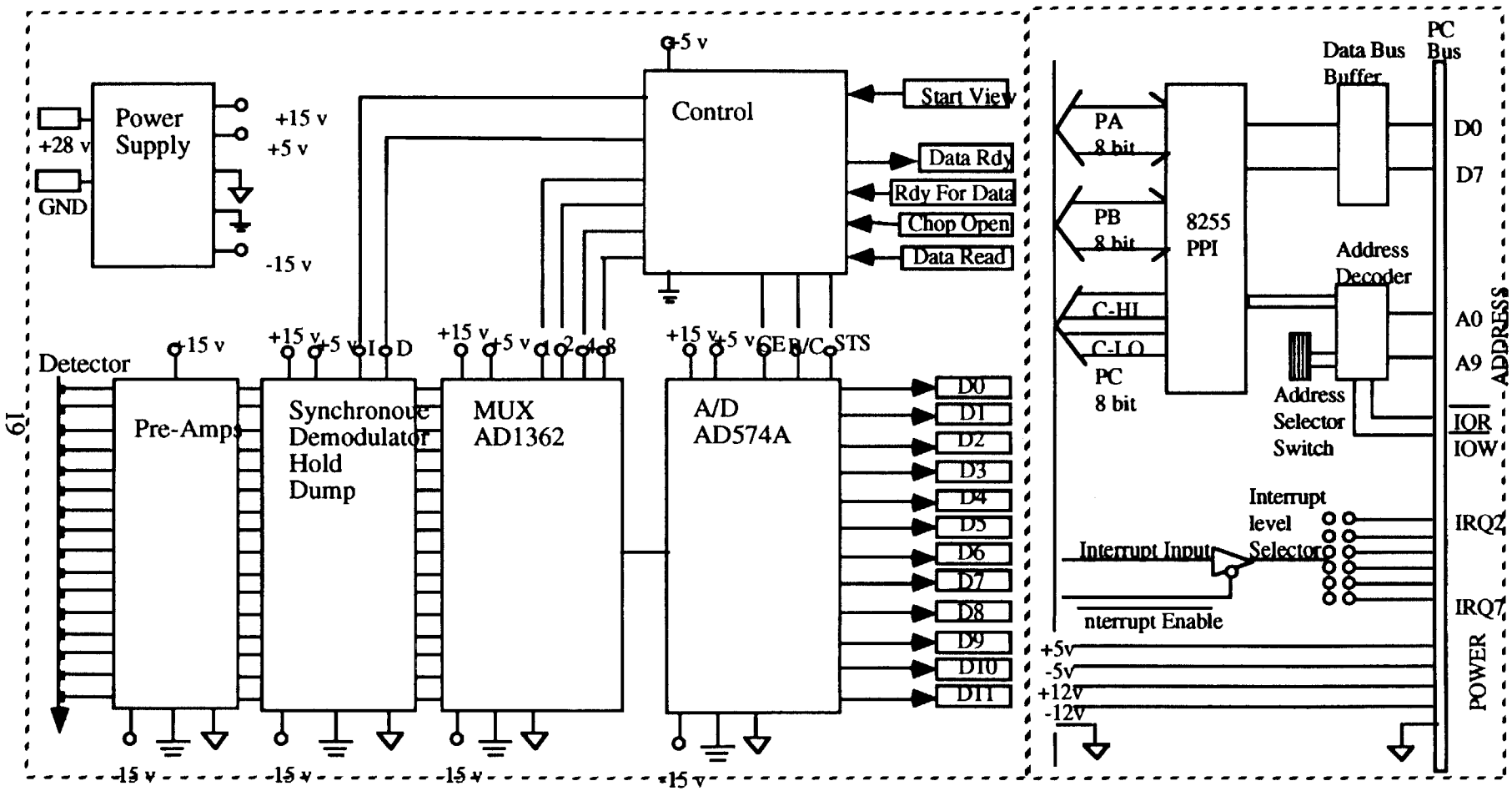

Detector Electronics by ITT/ACD

PIO Plugged in IBM/PC Data Acquisition

Fig. 3.7. MOES laboratory prototype electronics and data acquisition.

3.6 MOES Detector Subsystem Design and Development

A HgCdTe linear array with 16 elements is needed for the 16 MOES tropospheric temperature sounding channels. It can be seen from the kaleidoscope and cone assembly that there is not much room for the detector array around the apex of the cone, so a special mounting plate need to be designed. This mounting plate will serve as the heat sink for the detector array and also the interface between the array the kaleidoscope and cone assembly. The design and characteristics of the array are shown in Fig. 3.6.

3.7 MOES Electronics and Data Acquisition

The electronics for the 16 channel MOES laboratory prototype is designed by ITT/ACD. A functional diagram of the MOES electronics is shown in Fig. 3.7. Instrument control and data acquisition will be accomplished with a 386/33 PC.

4.0 MOES SYSTEM TEST AND CALIBRATION

4.1 Test Set-up

As shown in Fig. 4.1, the testing set-up includes infrared sources (tunable diode laser or blackbody), optical chopper, monochromator, adjustable reflecting mirror, MOES and LN2 dewar, a temperature sensor, MOES electronics, the vacuum system, the cryogenic system, and an IBM compatible PC to control the tunable diode laser (TDL) system, the monochromator, and the MOES data acquisition.

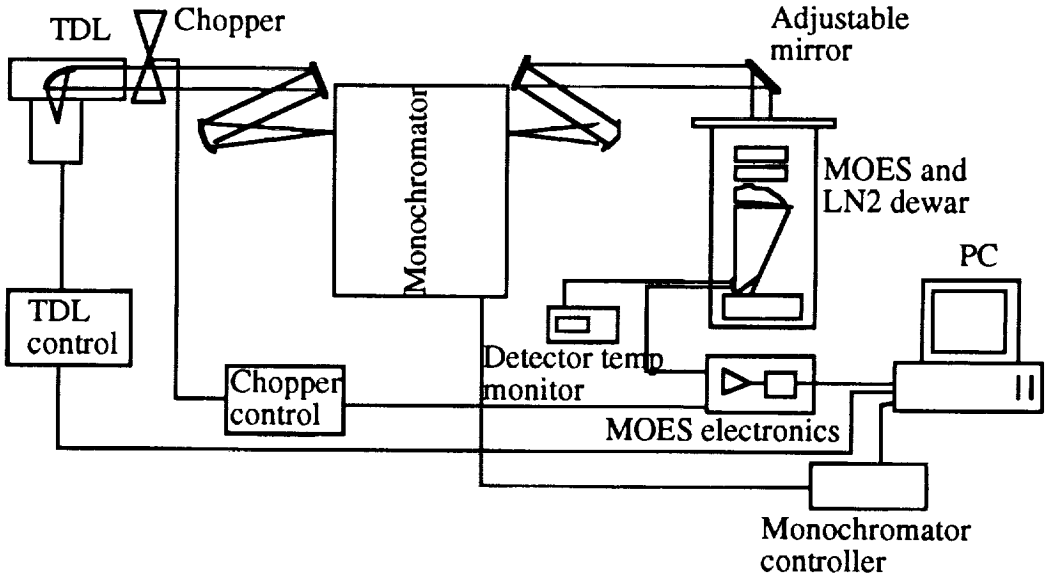

Fig. 4.1 MOES laboratory prototype test and calibration set-up.

4.2. Broad-Band Source Test

MOES system response was first tested with an uncollimated beam from a 1000 °C black body source. Result is shown in Fig. 4.2. From this test we can determine the detector response uniformity over 14 channels as well as the detector sensitivity (channel 15 and 16 are incorrectly connected by the detector manufacturer).

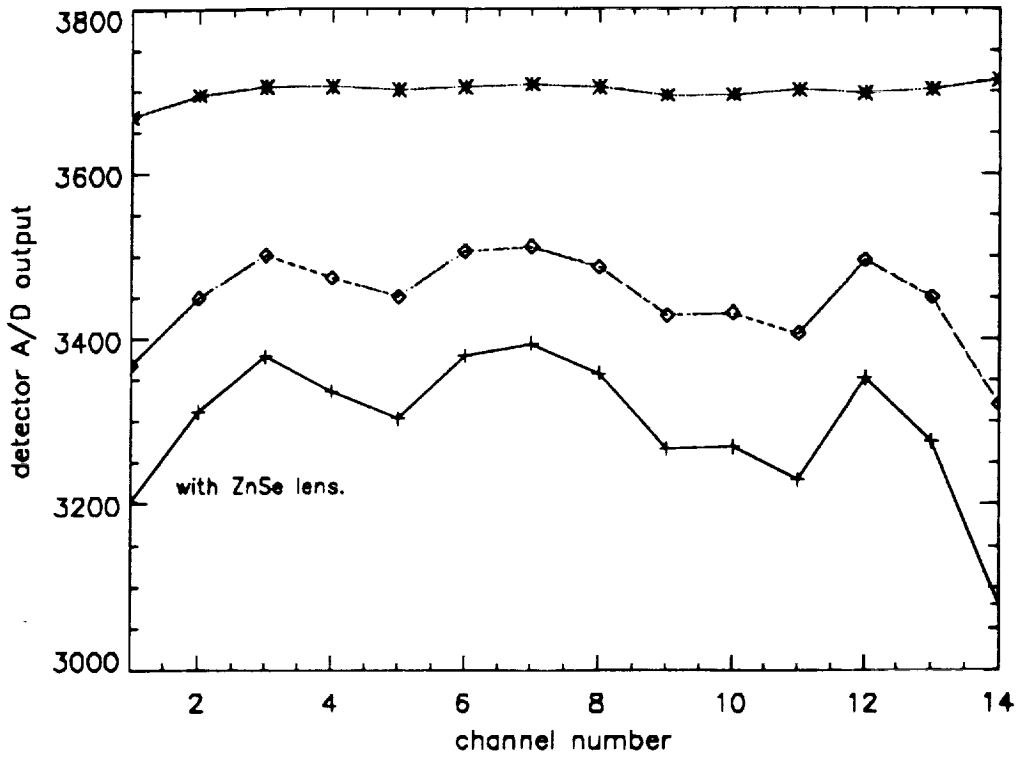

Fig. 4.2 MOES system test using a 1000 degree blackbody. *: source blocked; ◇: blackbody source without collimating lens; +: with lens (partially collimating beam).

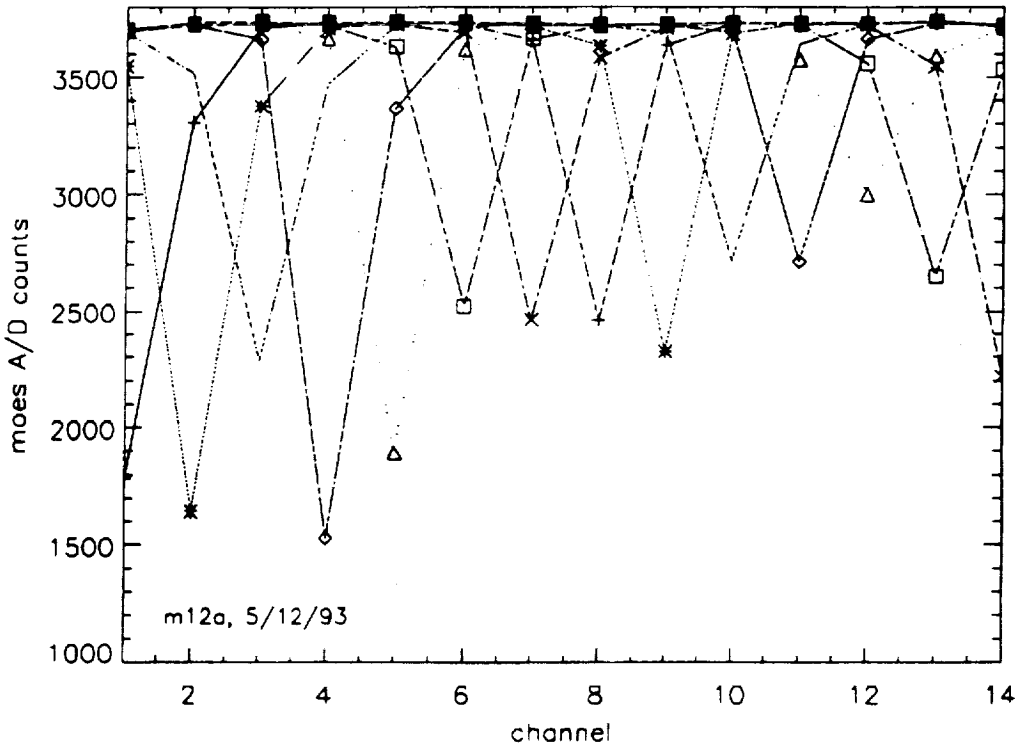

Fig. 4.3. MOES test without etalon and filter using TDL as monochromatic source. The laser beam from TDL is focused on one element each time by adjusting the adjustable mirror.

4.3. Lens-Kaleidoscope-Cone-Detector Test

The next step in the MOES test and calibration is to remove the MOES filter and the etalon from the system and test the rest of the system using the collimated Tunable Diode Laser (TDL) beam. The monochromator (Acton Research SP-500) was used to isolate a single mode of the laser. However when the monochromator was set at the mirror position instead of grating position, all TDL modes can pass through. The laser beam direction can be changed by quantitatively control the orientation of the reflecting mirror so that the beam can be focused on different channels of MOES detector. Ideally, this should be replaced by a diffuser, but using a Lambertian diffuser would lose so much signal that MOES cannot have high enough signal to noise. Therefore it is necessary to design a narrow angle diffuser. The results of this test are shown in Fig. 4.3. Note that the non-uniformity was not only due to the difference among the elements but also due to the imperfect illumination which was inevitable using a collimated source. When the diffused source is available, this problem will be eliminated.

4.4. MOES Filter Test Using FTIR

We conducted two tests on MOES narrow band filter using Bomem DA8 FTIR instrument with different resolution under room temperature. The low resolution (2 cm^{-1}, Fig. 4.4) test result is similar to the manufacturer's data (715 cm^{-1} to 729 cm^{-1} pass band FWHM under room temperature). However, the high resolution test (0.1 cm^{-1}, Fig. 4.5) indicated that the filter has channel spectrum, which means that the filter acts as a solid Fabry-Perot etalon. This result is consistent with the previous filter test using TDL. This channel spectrum is due to the parallelism of the Ge filter substrate. The substrate should be wedged to avoid multiple reflection between its two surfaces. The later results indicate that this channel spectrum (oscillation) of the MOES filter response curve does affect the total instrument function of MOES system as the spectral resolution of MOES is 0.06 cm^{-1}, which is narrower than the free spectral range of the filter oscillation (0.31 cm^{-1}).

4.5. System Calibration (without filter)

MOES system spectral calibration was carried out using the TDL system. Computer controlled TDL scans were accompanied by the controlled monochromator scans to follow the same laser mode. At this stage the filter was removed. For the time being the laser beam we use was collimated and was focused on one detector element each time. This requires a great deal of alignment work. We are currently investigating ways to get a narrow angle diffused laser beam so that we can get relatively uniform illumination on all 16 channels. The test results are shown in Fig. 4.6 through Fig. 4.10. Some channels have asymmetric Airy peaks due to imperfect illumination. The peak wavenumbers of the response curves for all channels (shown in Fig. 4.11) agree with the expected parabolic curve quite well. A narrow angle diffuser is necessary for the MOES radiometric calibration.

4.6. The Complete MOES System Calibration

Everything in the setup was the same as in section 4.5 except the MOES filter is in place. The results (Fig. 4.12 to Fig. 4.23) indicates that significant oscillations in signal intensity exist among different channels. Also some sudden variations occur in the Airy peaks of certain channels. These must be caused by the oscillation in the filter response. It is rather difficult to correct this filter effect by including the oscillation in the instrument function because the filter response is highly temperature dependent (the response curve will shift to a different spectral range when temperature changes). In order to do this, first we have to measure the filter transmission under a precisely controlled and accurately measured temperature near liquid nitrogen temperature. Secondly, we need to operate the MOES system exactly under the same temperature. Since the MOES dewar temperature is always varying and the thermistor measures the temperature near the detector instead of the filter, it is difficult to satisfy the second condition. Therefore we believe a new filter should be made in order to get an accurate instrument function measurement. The peak wavenumber for each channel is shown in Fig.

4.24. System finesse was measured as 25 to 28 (for different peaks). A bit lower than etalon finesse measured before (33 to 35). The factors that contributes to the finesse degradation include finite detector element area, system aberration, etc.

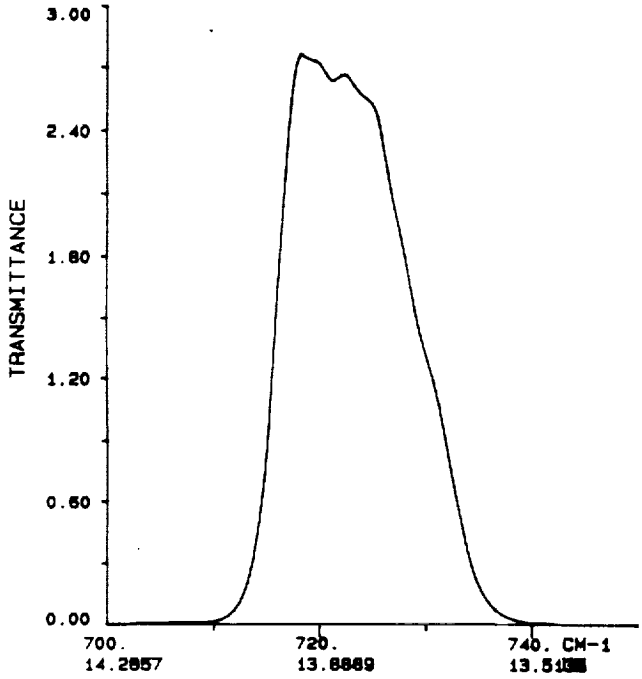

Fig. 4.4. MOES filter measurement using Bomem DA8 with a spectral resolution of 2.0 cm^{-1}, the transmission scale here is arbitary. The peak transmission of the filter is 75%.

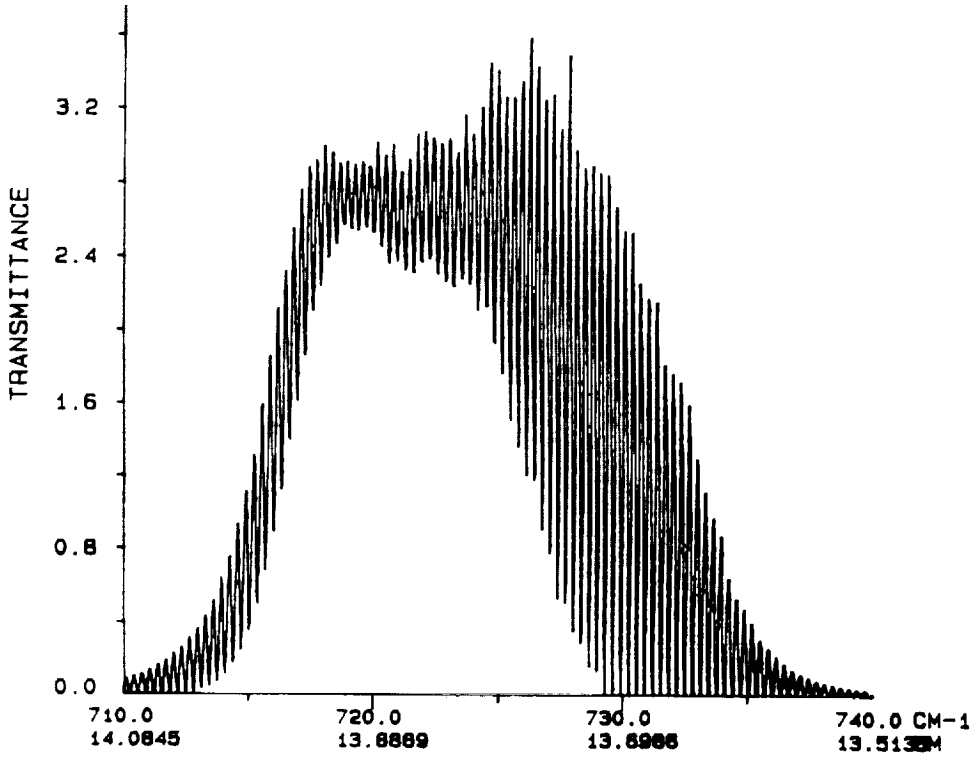

Fig. 4.5. MOES filter measurement using Bomem DA8 with a spectral resolution of 0.1 cm^{-1}.

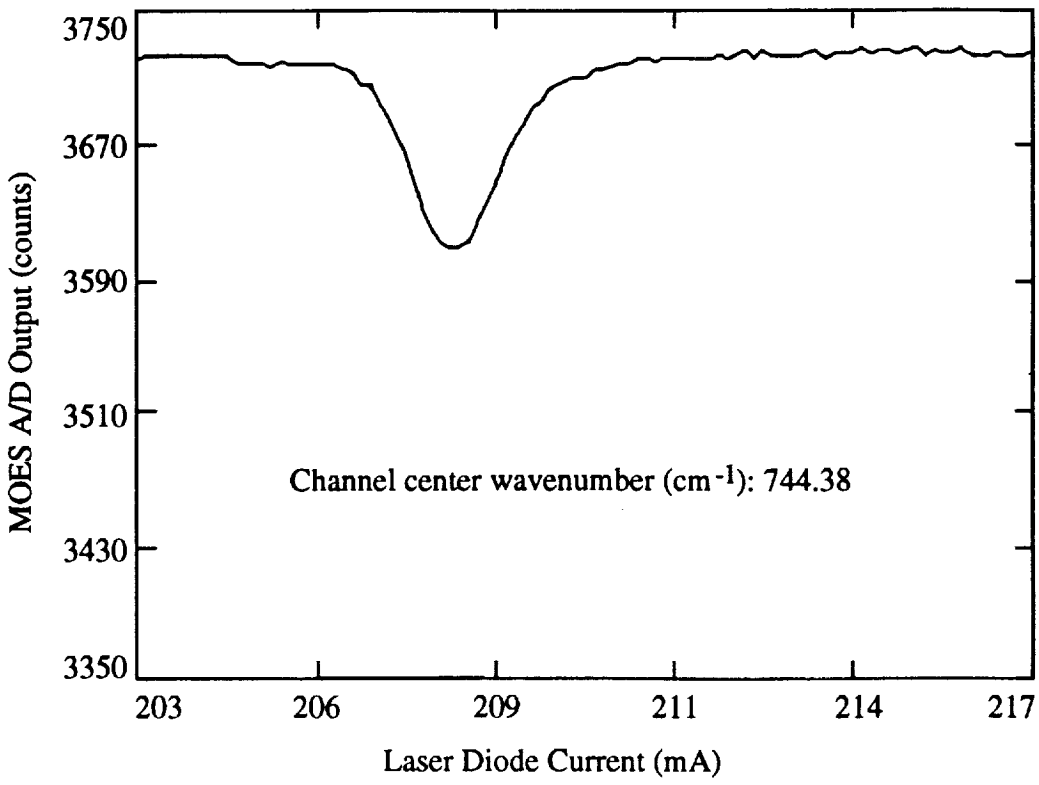

Fig. 4.6. MOES system test without the band blocking filter. Channel #6.

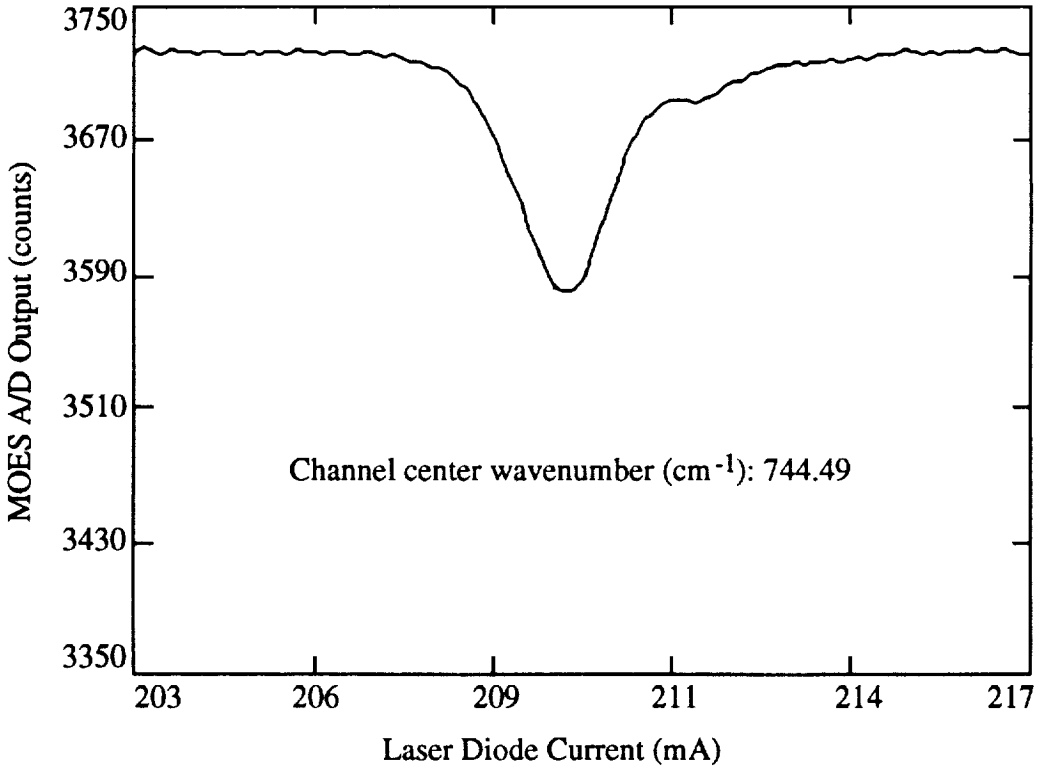

Fig. 4.7. MOES system test without the band blocking filter. Channel #7.

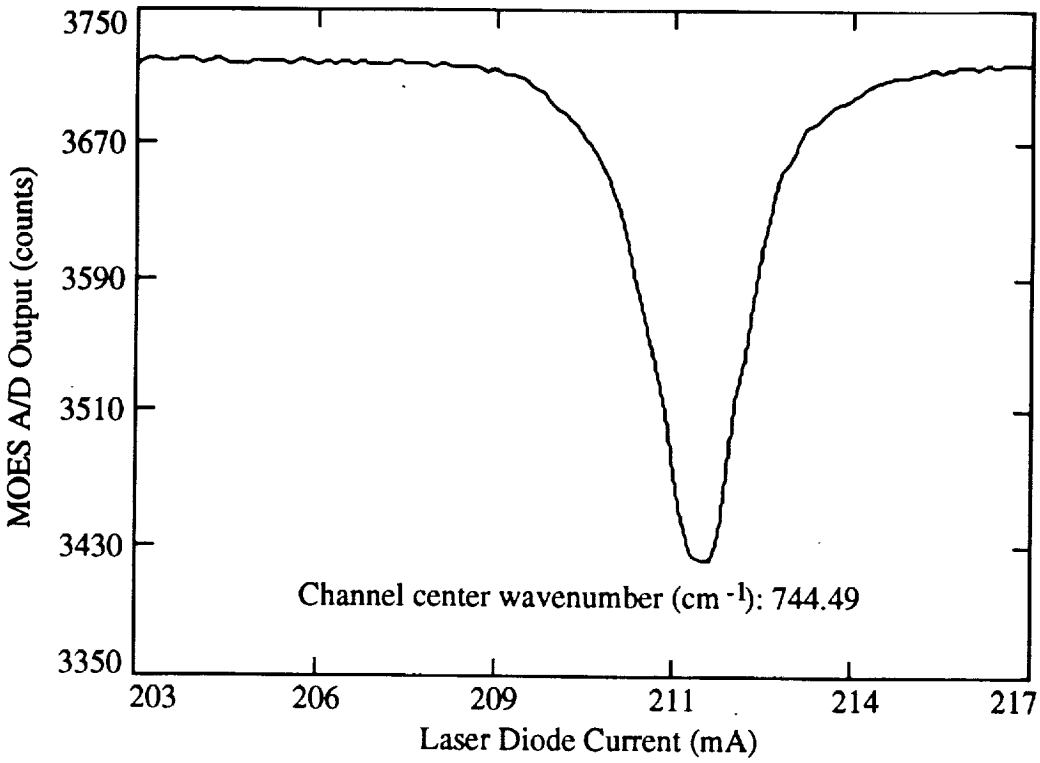

Fig. 4.8. MOES system test without the band blocking filter. Channel #8.

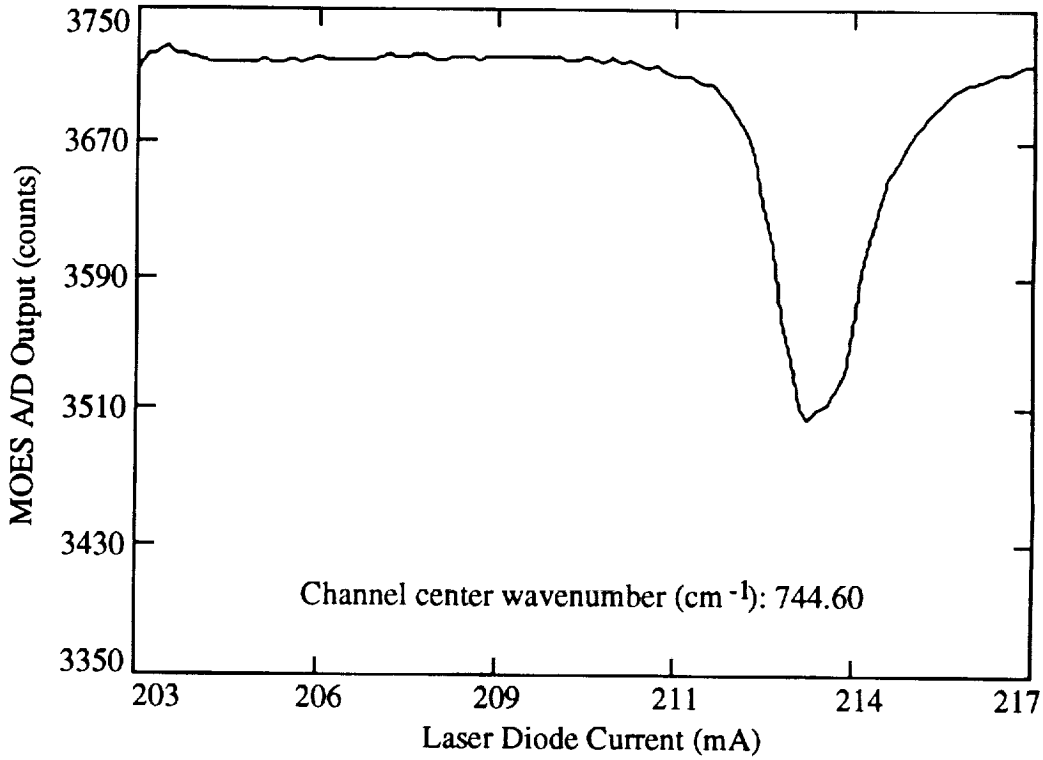

Fig. 4.9. MOES system test without the band blocking filter. Channel #9.

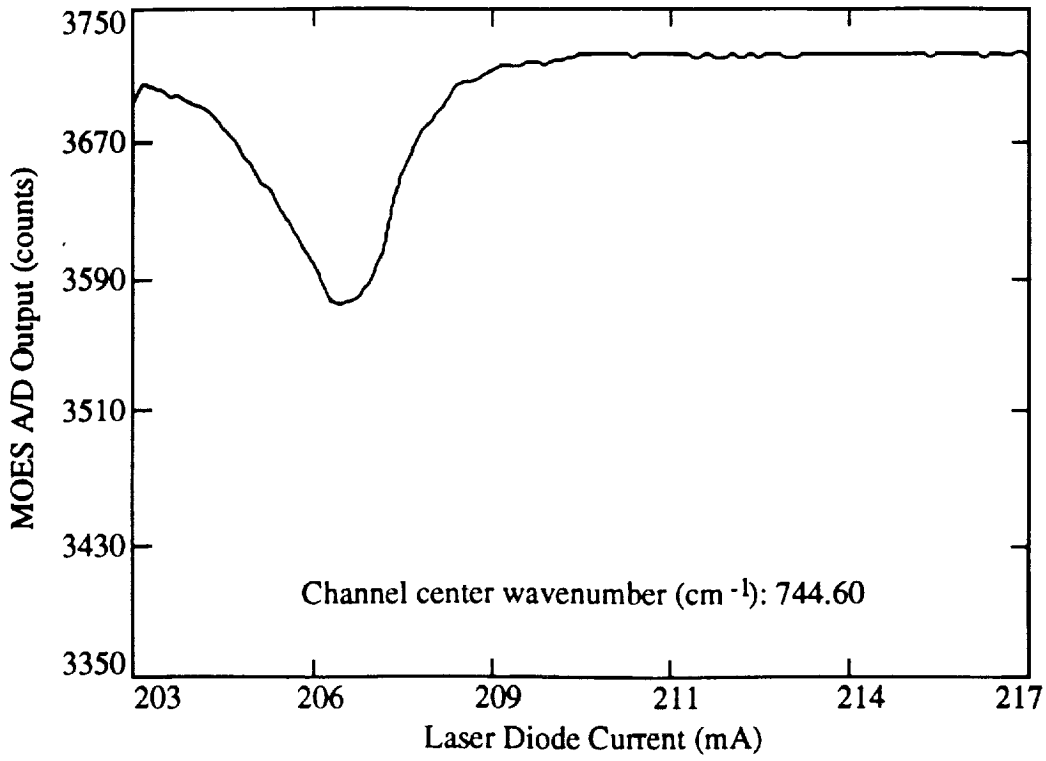

Fig. 4.10. MOES system test without the band blocking filter. Channel #10.

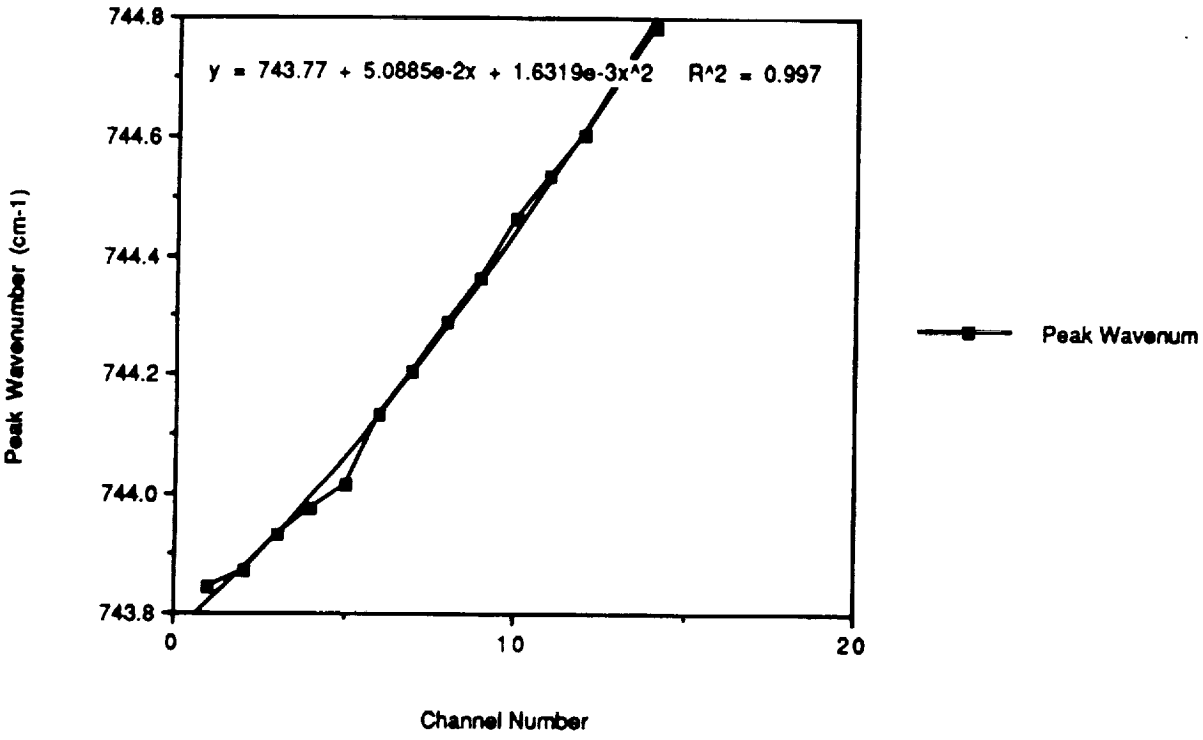

Fig. 4.11. MOES peak response wavenumber for each channel without the band blocking filter.

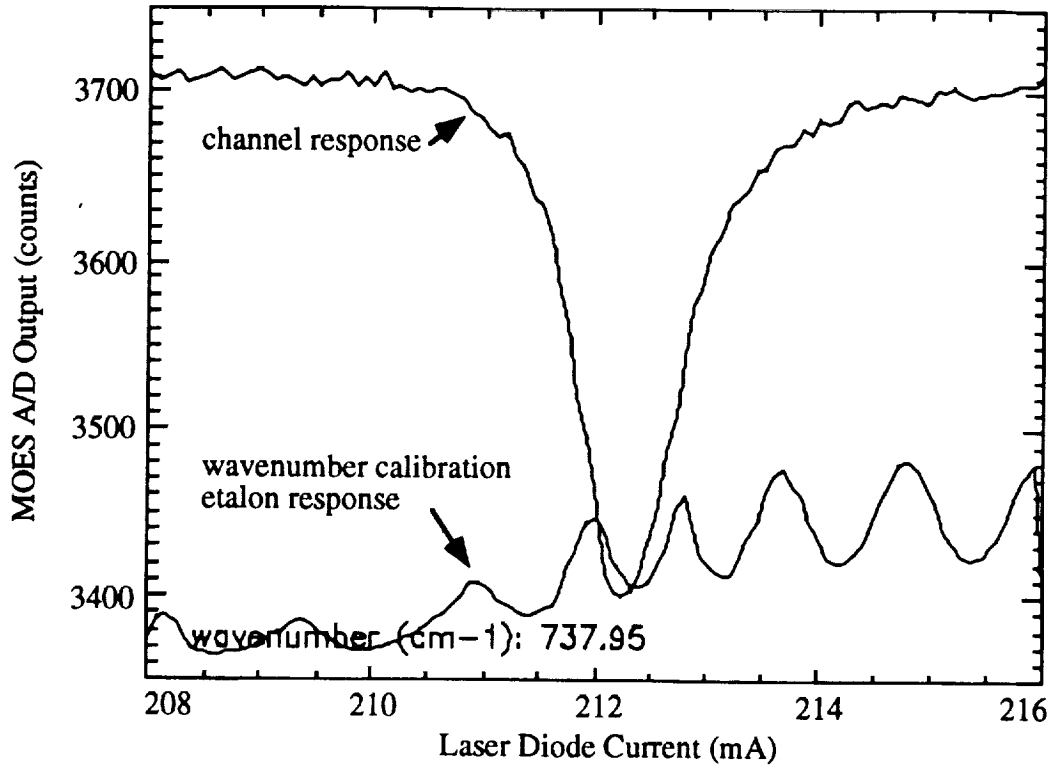

Fig. 4.12. MOES channel response measurement with the TDL. Channel #1.

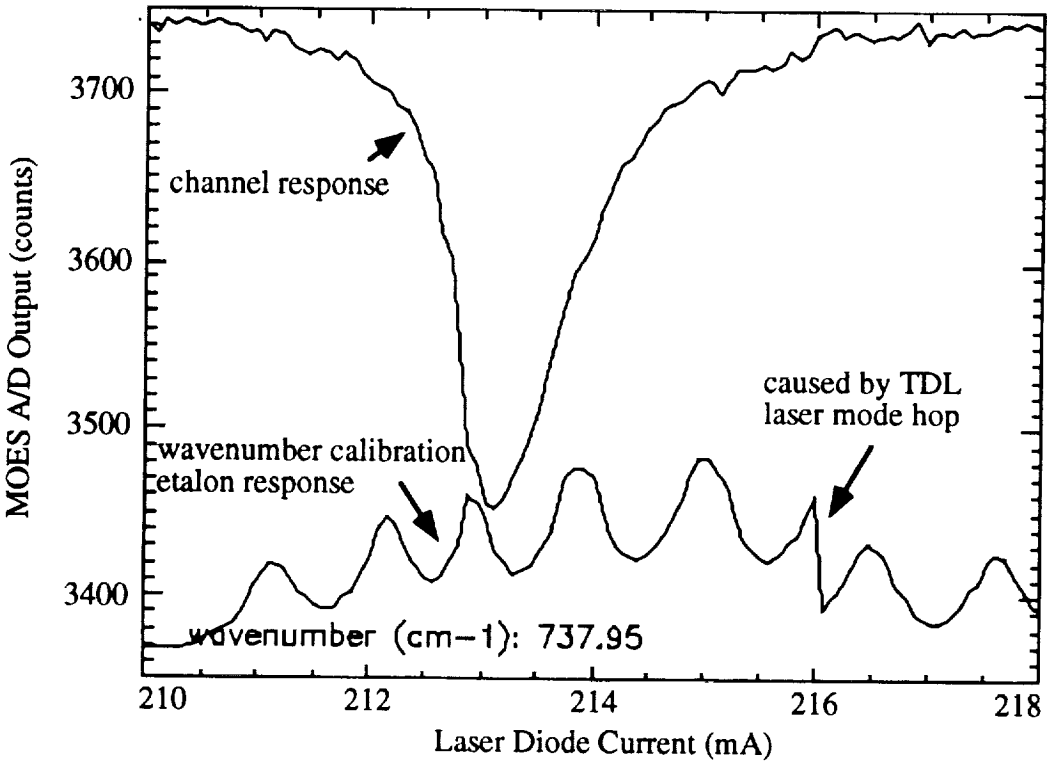

Fig. 4.13. MOES channel response measurement with the TDL. Channel #2.

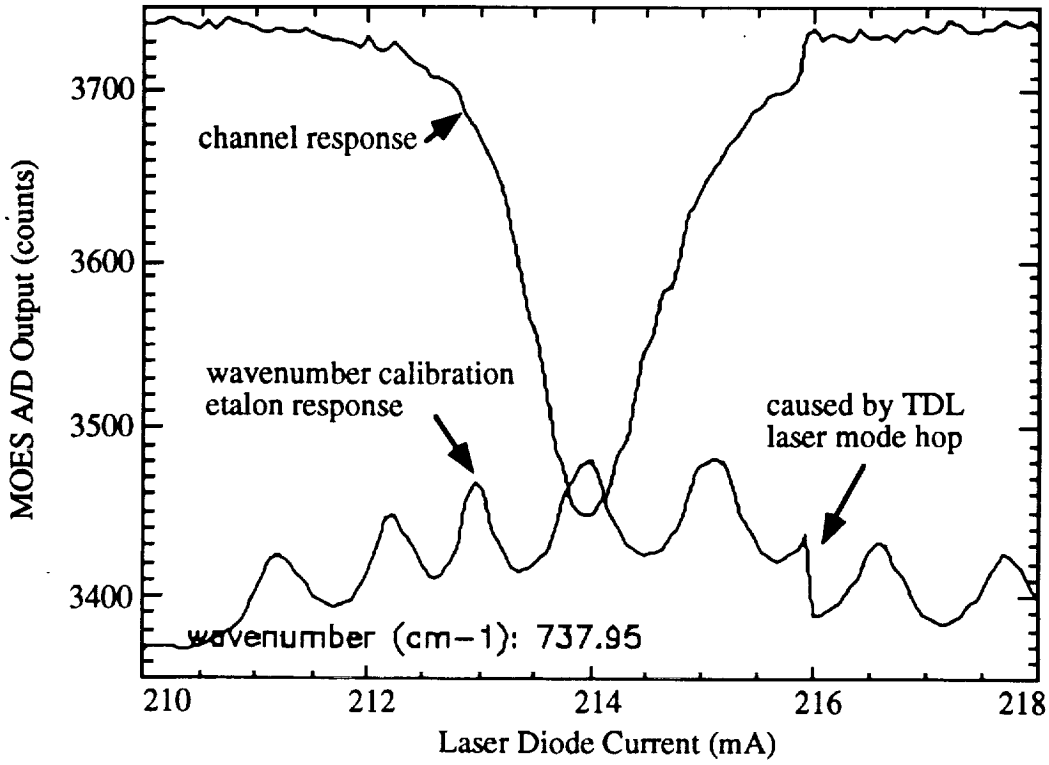

Fig. 4.14. MOES channel response measurement with the TDL. Channel #3.

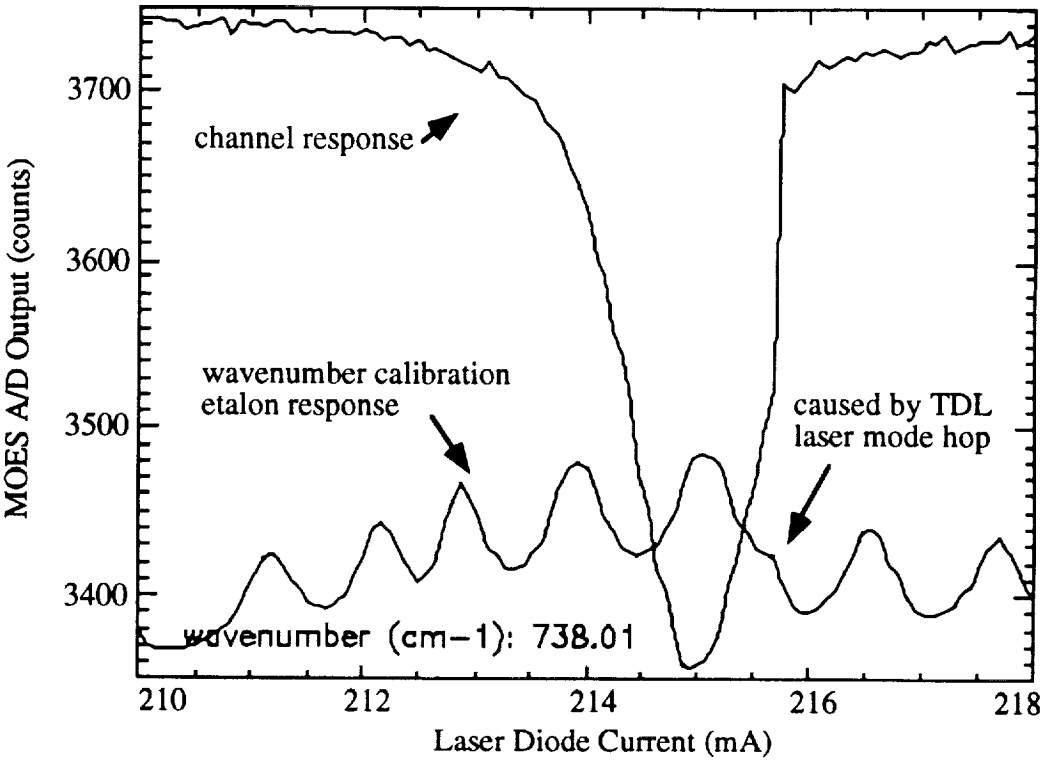

Fig. 4.15. MOES channel response measurement with the TDL. Channel #4.

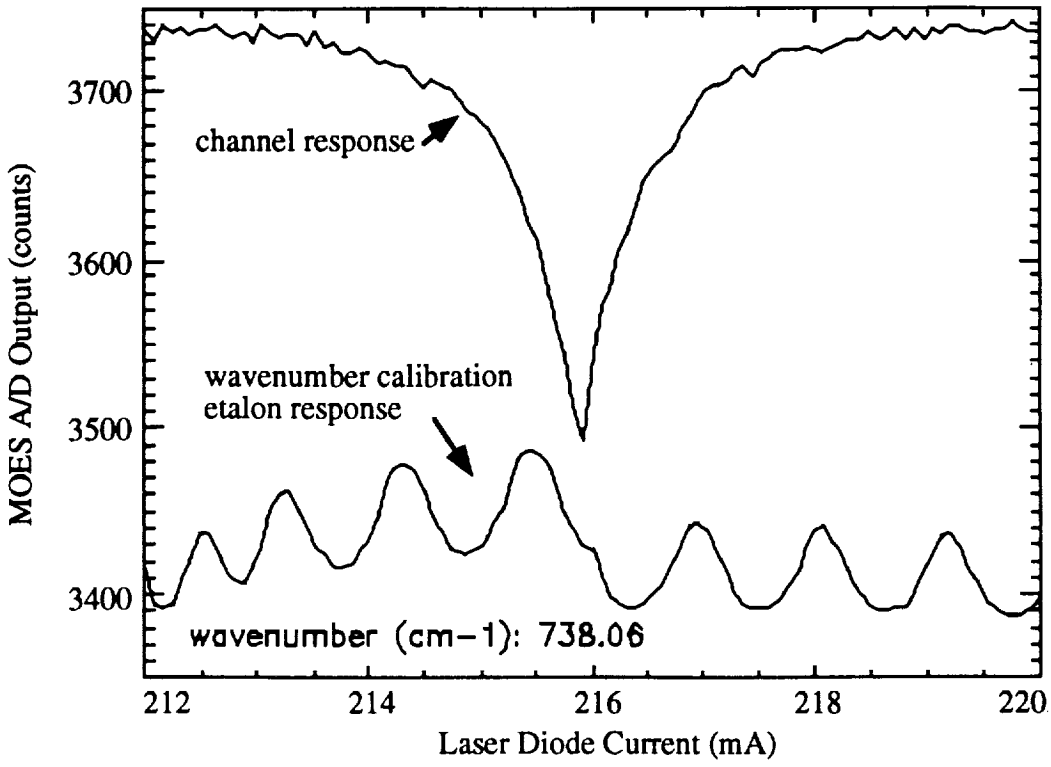

Fig. 4.16. MOES channel response measurement with the TDL. Channel #5.

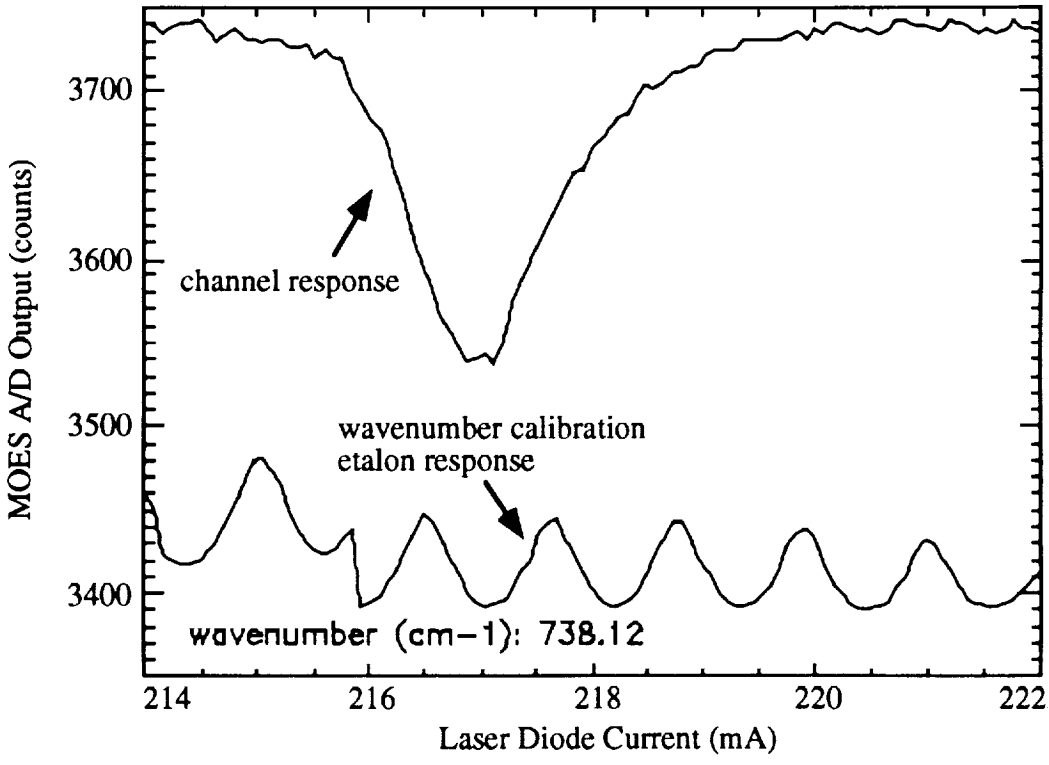

Fig. 4.17. MOES channel response measurement with the TDL. Channel #6.

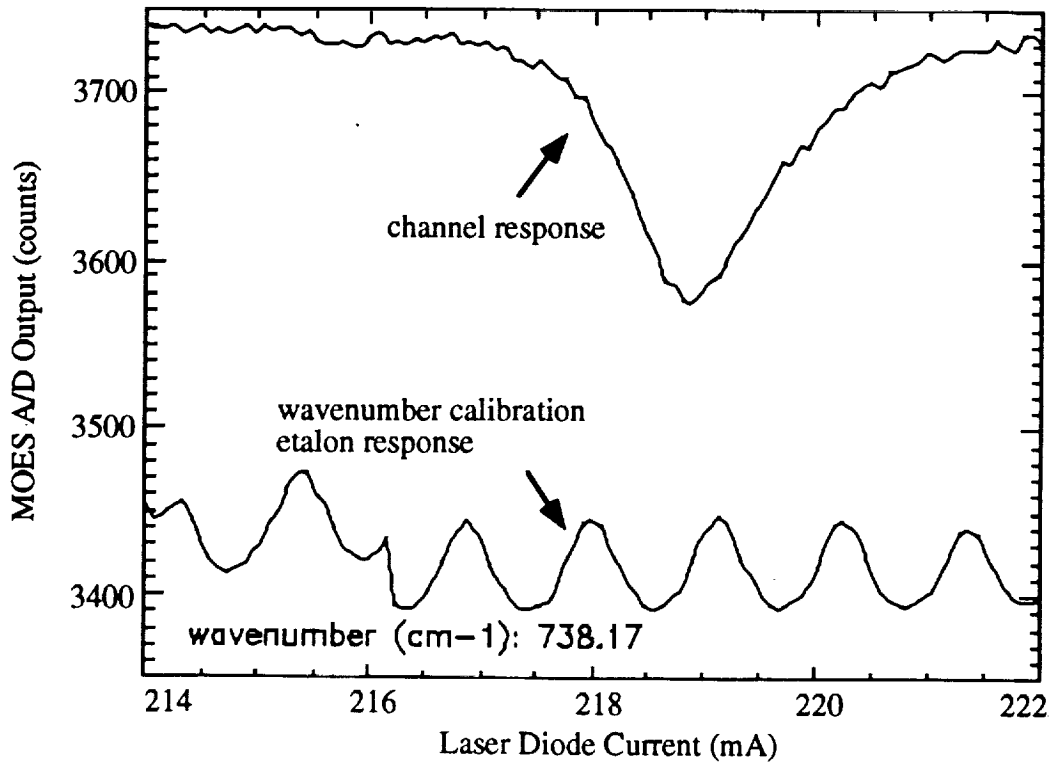

Fig. 4.18. MOES channel response measurement with the TDL. Channel #7.

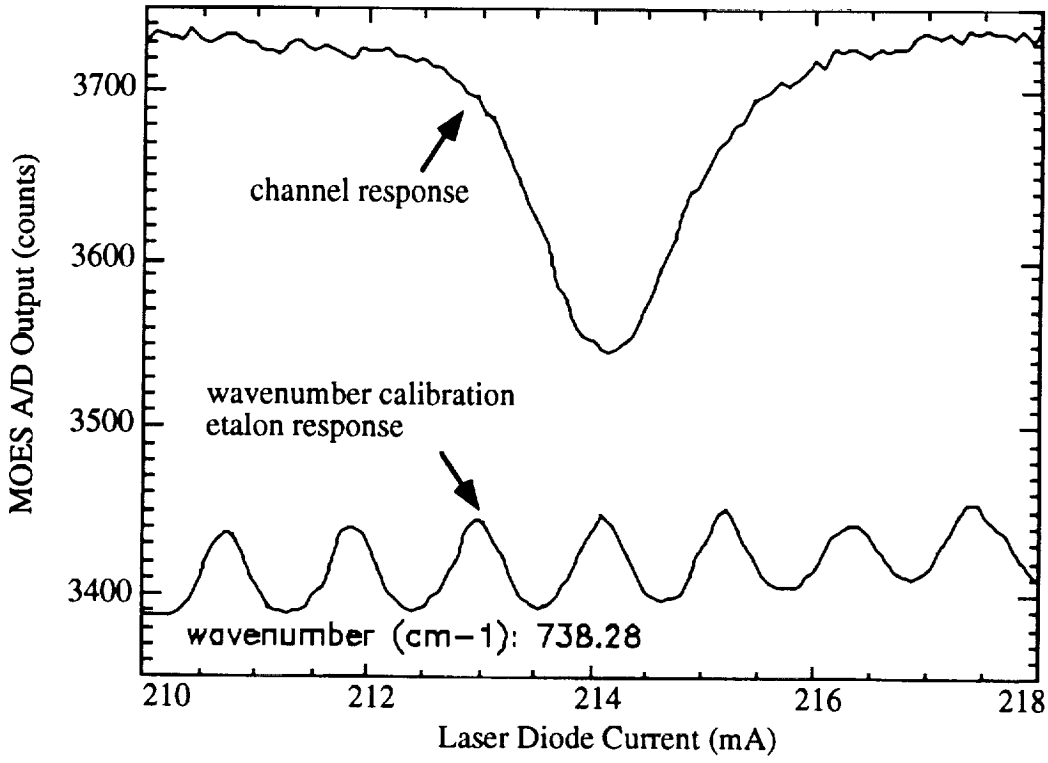

Fig. 4.19. MOES channel response measurement with the TDL. Channel #8.

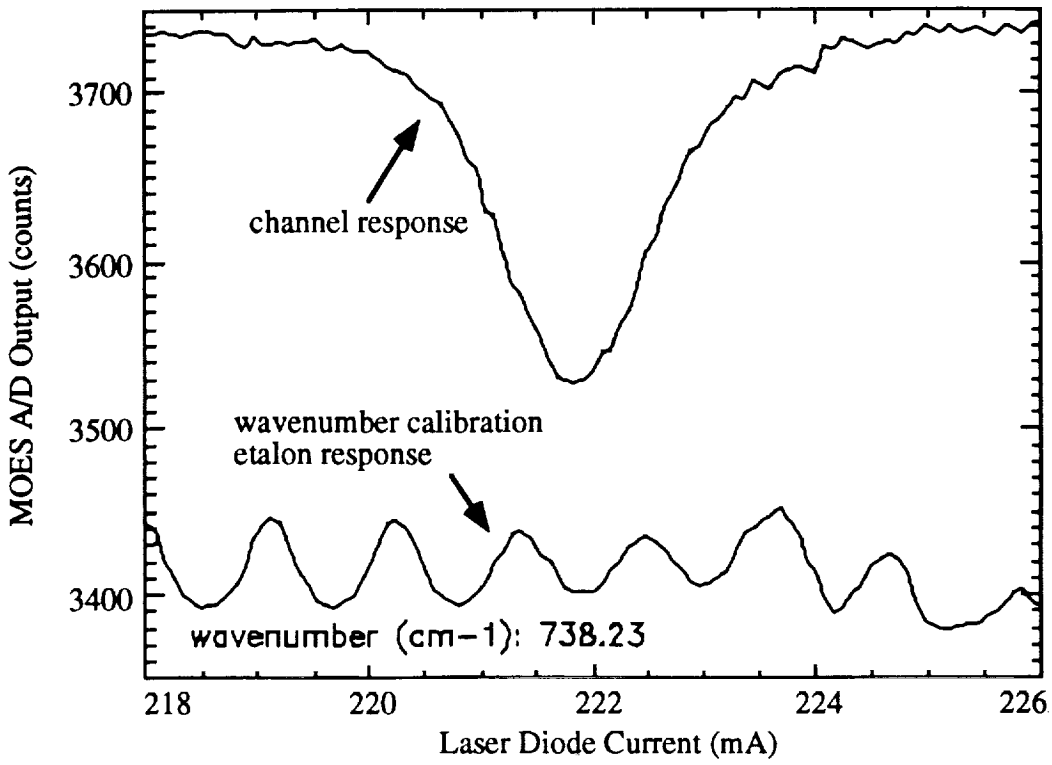

Fig. 4.20. MOES channel response measurement with the TDL. Channel #9.

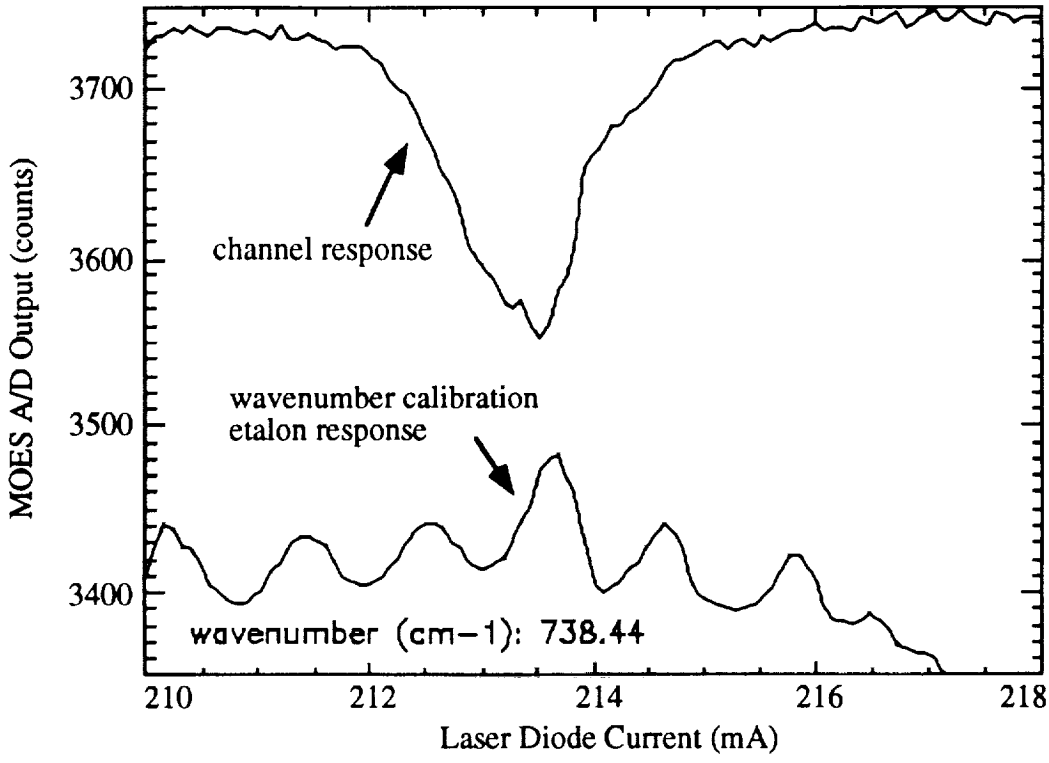

Fig. 4.21. MOES channel response measurement with the TDL. Channel #10.

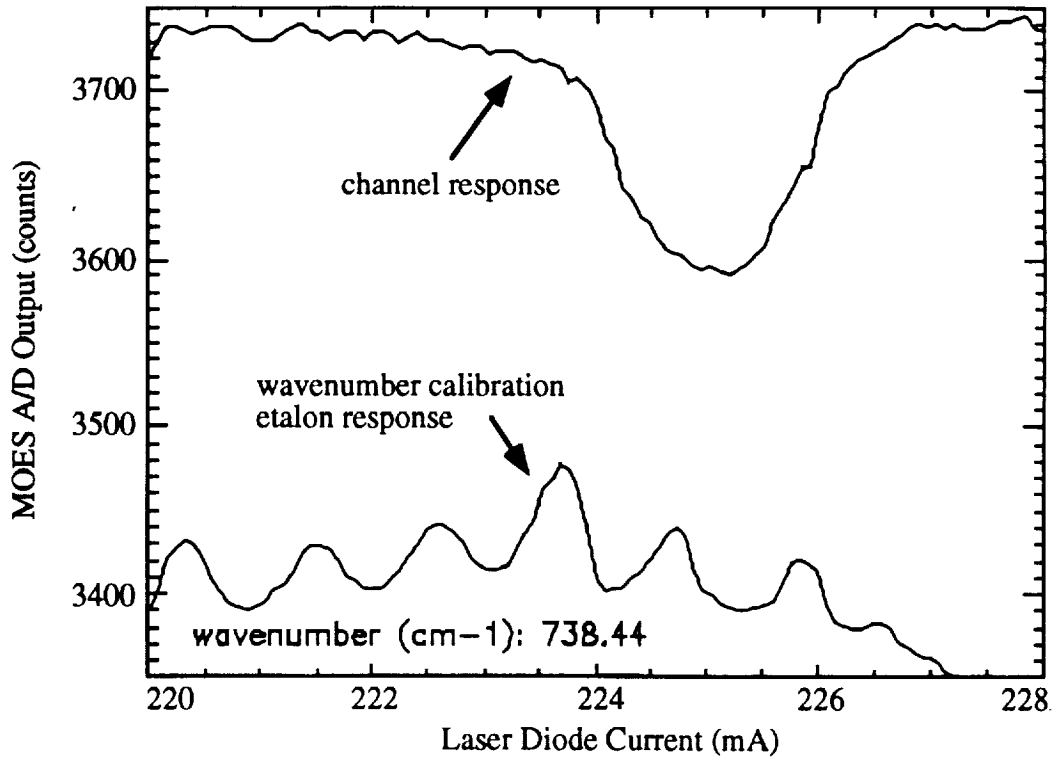

Fig. 4.22. MOES channel response measurement with the TDL. Channel #11.

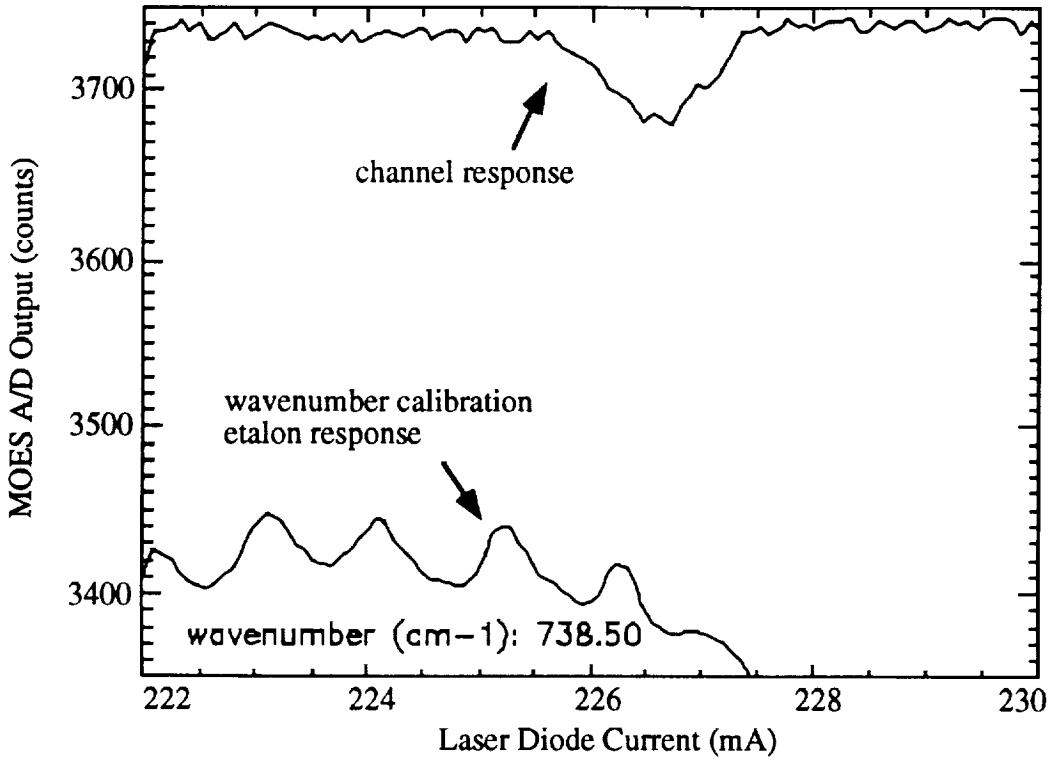

Fig. 4.23. MOES channel response measurement with the TDL. Channel #12.

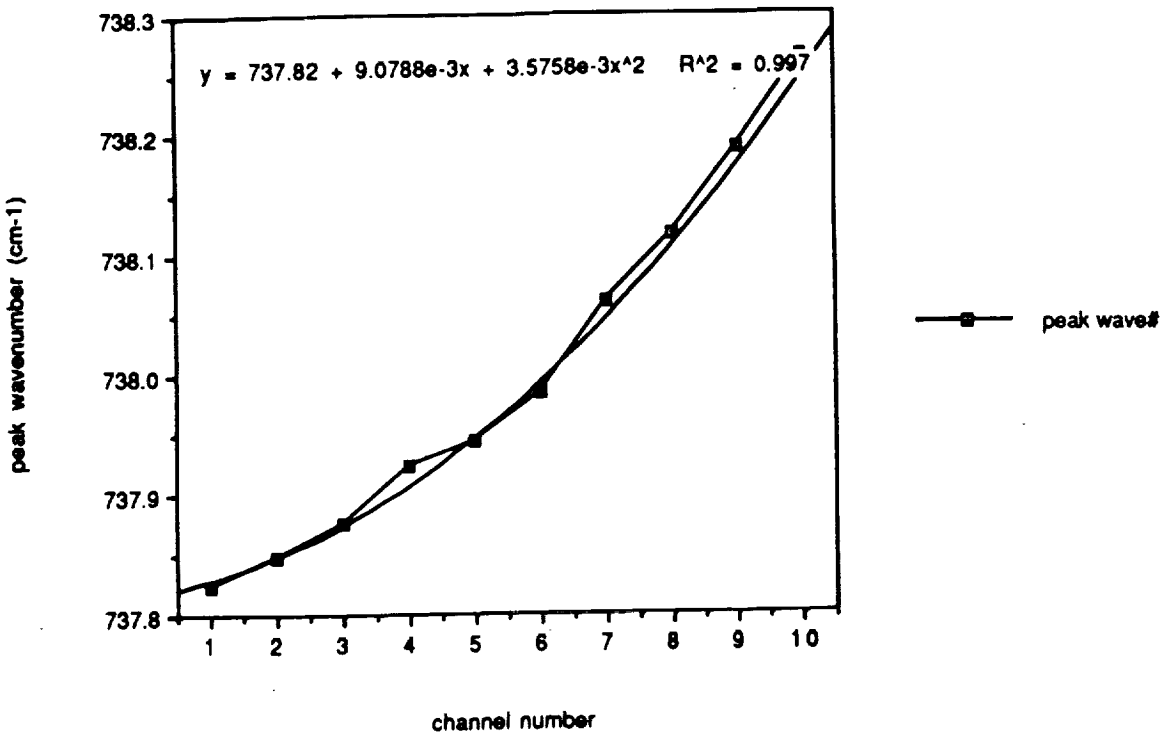

Fig. 4.24. MOES system response peak wavenumber .vs. channel number. This measurement provides the center wavenumbers of channels 1 - 10.

5.0 MOES BALLOON FLIGHT GONDOLA DESIGN

5.1. Gondola Design

We have examined the possibility of using an existing gondola from the High Resolution Doppler Imager (HRDI) experiment for a possible balloon flight of MOES. The conclusion is that the HRDI gondola is too big and heavy for a small instrument like MOES, it is better to design and construct a smaller gondola for MOES balloon flight demonstration. The schematic diagram of the gondola lower level, upper level, and side view are shown in Fig. 5.1 and Fig. 5.2.

5.2. MOES Instrument and Gondola Weight and Dimensions

The weight and dimensions of the MOES instrument and gondola are summarized in Table 5.1.

6.0 SUMMARY

The MOES development effort at SPRL shows that MOES is technically feasible, a prototype has been developed and tested. The imaging quality and design tolerance of the critical CLIO have been studied. A gondola design for a possible MOES balloon flight has been conducted. The results of this research project and experience gained will be valuable in the quick implementation of a MOES balloon flight in the future.

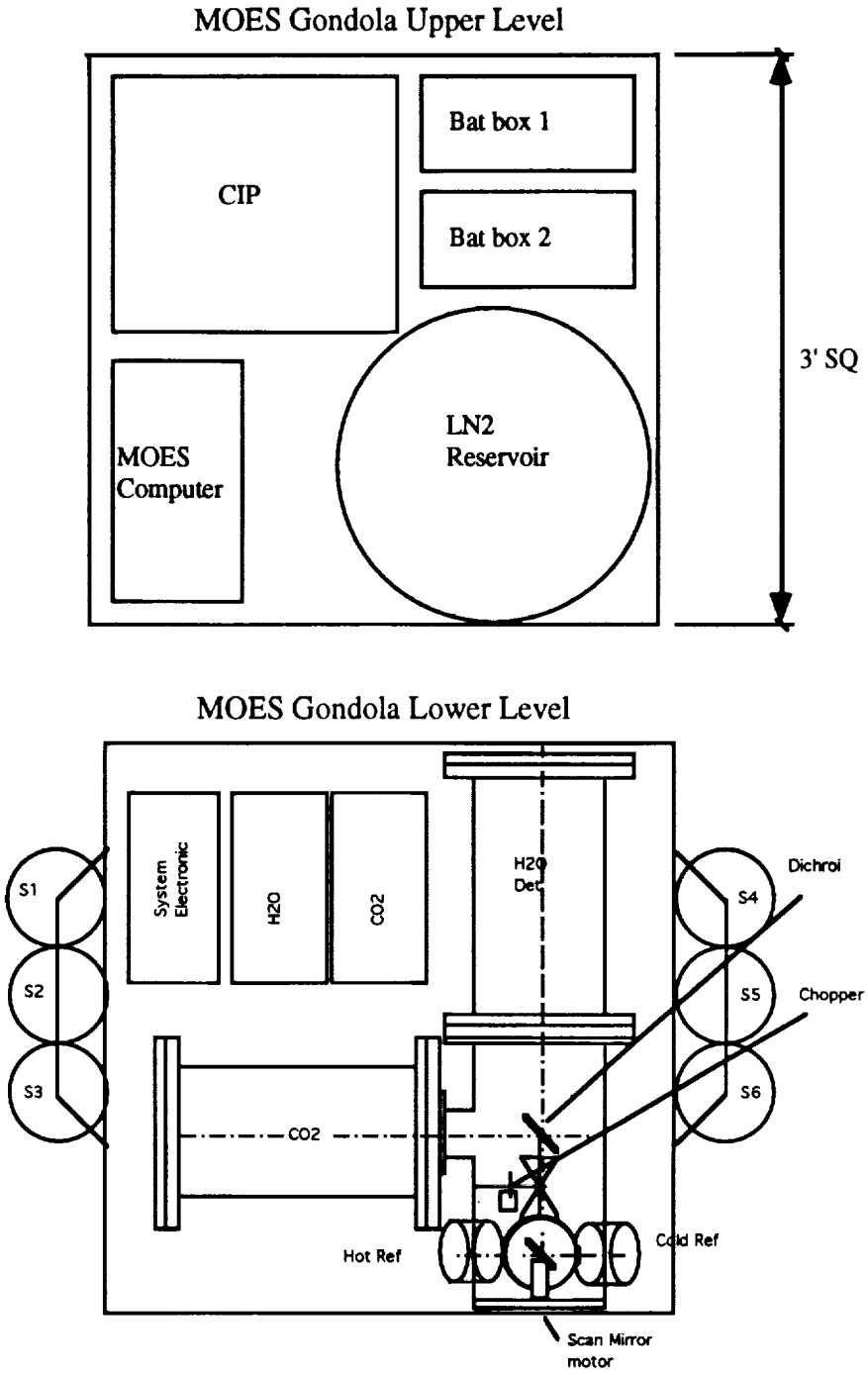

Fig. 5.1. Schematic diagram of the MOES balloon flight gondola lower level and upper level.

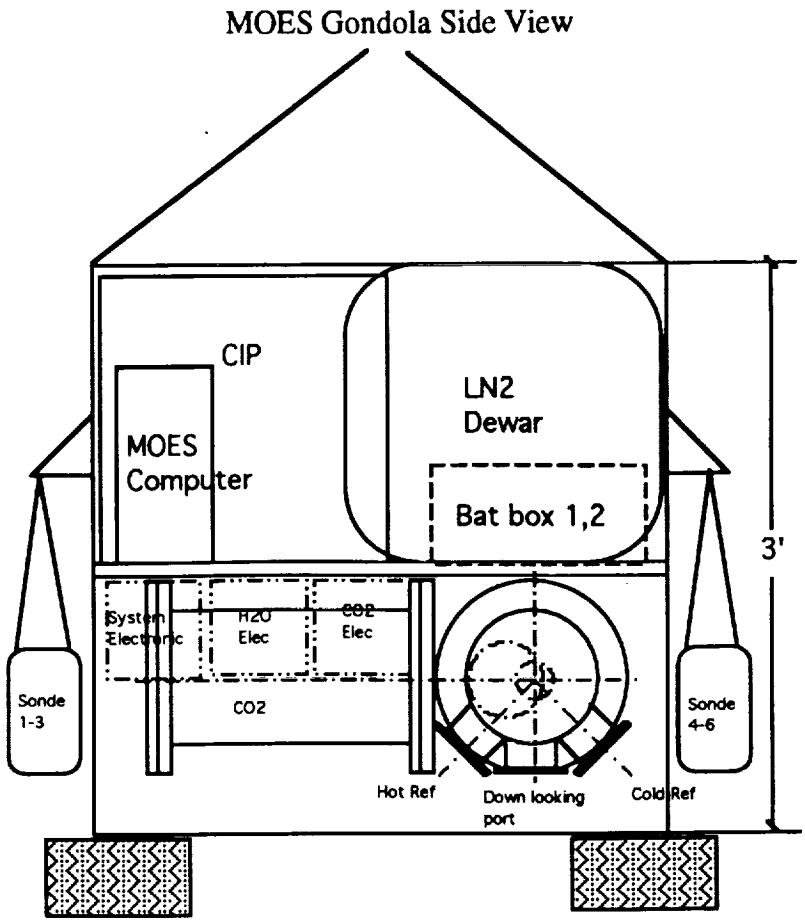

Fig. 5.2. MOES gondola side view.

Table. 5.1. MOES Balloon Instrument and Gondola Dimensions and Weigh

Item	LxWxH (in.)	Weight (lbs.)	Provided by
Gondola	36x36x36	140	SPRL
CIP	15x19x18	60	NSBF
Battery Box	8x12x8	20x2	NSBF
LN2 Reservoir	17" Dia.x24.1 H	84 (full)	AIRCO
CO_2 Band	12" Dia.x18 L	90	ITT
H_2O Band	12" Dia.x18 L	90	ITT
Scan/Ref Housing	12" Dia.x15 L	25	SPRL
Scan Mirror Assy	3" Dia. x 2 L	2	SPRL
Relay Optics Assy	2" Dia. x 4" L	1	SPRL
Chopper Assy	4" Dia. x 2" L	1	SPRL
Cold Ref	3" Dia. x 3" L	1	SPRL
Hot Ref	3" Dia. x 3" L	1	SPRL
H_2O Band Electronics	12x6x6	4.5	ITT
CO_2 Band Electronics	12x6x6	4.5	ITT
Detector Harness		2.0	SPRL
System Electronics	12x6x6	20	SPRL
Chopper elec.			
Scan mirror elec.			
Power supplies			
House Keeping			
Computer (hermetic)	14x14x6	25	SPRL
Cryogenic System		15	SPRL
Video Camera	6" Dia. x12 L	10	SPRL
Radiosondes	6" Dia. x18 L	3x6	TBD
Total Weight: 634 lbs.			

REFERENCE

Abel, P. G., P. J. Ellis, J. T. Houghton, G. E. Peckham, C. D. Rogers, S. D. Smith, and E. J. Williamson, "Remote Soundings of Atmospheric Temperature from Satellites: II. The Selective Chopper Radiometer for Nimbus D,"*Proc. Roy. Soc. Lond.*, Series A. **320**, pp. 35-55, 1970.

Anderson, G. P., J. H. Chetwynd, S. A. Clough, E. P. Shettle, and F. X. Kneizys, "AFGL Atmospheric Constituent Profiles (0 - 120 km)," *AFGL-TR-86-01110*, May, 1986.

Born, M., and E. Wolf, *Principle of Optics*, 5th ed., Pergamon Press, Oxford, 1975.

Jacquinot, P., "The Luminosity of Spectrometers with Prisms, gratings or Fabry-Perot Etalons," J. Opt. Soc. Am., **44**, pp. 761-765, 1954.

Koenig, E. G., "Performance of the HIRS/2 Instrument on TIROS-N," Remote Sensing of Atmosphere and Oceans, pp. 67-91, edited by A. Deepak, Academic, New York, 1980.

Koenig, E. W., "Requirements for the Next Generation Temperature and Moisture Sounders on the LEO Satellites", Private Communication, 1990.

Falbel, G., and D. Zink, "A Sequential Filter Radiometer for Sensing the Vertical Temperature Profile of the Earth's Atmosphere," *Proceedings of Joint Conference on Infrared Techniques*, I. E. R. E. (university of Reading), pp. 231-255, 1971.

Fleming, H. E., M. D. Golfberg, and D. S. Crosby, "Minimum Variance Simultaneous Retrieval of Temperature and Water Vapor from Satellite Radiance Measurements," *Reprints, Second Conf. on Satellite Meteorology/Remote Sensing and Appl.*, Williamsburg, Virginia, pp. 20-23, 1986. [American Meteorological Society, 45 Beacon St., Boston, MA 02108].

Fleming, H. E., "A Physical Retrieval Algorithm for Obtaining Microwave Soundings," *Passive Microwave Observing from Environmental Satellites: A Status Report Based on NOAA's June 1-4, 1987 Conference in Williamsberg, Virginia, NOAA Tech. Rep. NESDIS 35*, pp. 33-45, 1987.

Fleming, H. E., "Retrieval Simulation of MOES and HIRS/2 with the NOAA/NESDIS MVS Algorithm," Private Communications, 1990.

Hanel, R. A., B. Schlachman, F.D. Clark, C. H. Prokesh, J. B. Taylor, W. M. Wilson, and L. Chaney, "The Nimbus 3 Michelson Interferometer," *Appl. Opt.*, **9**, pp. 1767-1774, 1970.

Hays, P. B., T. L. Killeen, and B. C. Kennedy, "The Fabry-Perot Interferometer on Dynamics Explorer," *Space Sci. Inst.*, **5**, pp. 395-416, 1981.

Hays, P. B., "Circle to Line Interferometer Optical System," *Appl. Opt.*, **29**, pp. 1482-1489, 1990.

Nordberg, w., A. W. McCulloch, L. L. Foshee, and W. R. Bandeen, "Preliminary Results from Nimbus II," *Bull. Am. Meteorol. Soc.*, **45**, pp. 684-687, 1966.

Phillips, N., L. McMillin, A. Gruber, and D. Q. Wark, "An Evaluation of Early Operational Temperature Soundings From TIROS-N," *Bull. Am. Meteorol. Soc.*, **60**, pp. 1188 - 1197, 1979.

Smith, W. L., D. T. Hilleary, E. C. Baldwin, W. Jacob, H. Jacobwitz, G. Nelson, Soules, and D. Q. Wark, "The Airborne ITPR Brassboard Experiment," *NOAA Technical Report NESS 58*, Washington, D. C., March 1972.

Smith, W. L., H. M. Woolf, C. M. Hayden, D. Q. Wark, and C. M. McMillin, "The Tiros-N Operational Vertical Sounder," *Bull. Am. Meteorol. Soc.*, **60**, pp. 1177-1187, 1979.

Smith, W. L., H. M. Woolf, H. B. Howell, H. L. Huang, and H. E. Revercomb, "The Simultaneous Retrieval of Atmospheric Temperature and Water Vapor Profiles - Application to Measurements with the High Spectral Resolution Interferometer Sounder (HIS)," *RSRM'87: Advances in Remote Sensing Retrieval Methods*, edited by A. Deepak, H. E. Fleming, and J. S. Theon, pp. 189-202, A Deepak Publishing, 1989.

Vaughan, J. M., *The Fabry-Perot Interferometer: History, theory, Practice and Applications*, Adam Hilger, 1989.

Wang, J., Paul B. Hays, S. Roland Drayson, and Edward W. Koenig, "Multiorder Etalon Sounder (MOES): A New Technique for Passive High Resolution Atmospheric Temperature and Moisture Sounding from Satellite," *IEEE Trans. on Geo. and Remote Sensing*, Vol. **31**, No. 1, 1993.

Wang, J., " An Investigation on the Multiorder Fabry-Perot Interferometer as a Satellite-Borne High Resolution Atmospheric Temperature Sounder," Ph.D. Thesis, University of Michigan, 1990.

Wark, D. Q., and D. T. Hilleary, "Atmospheric Temperature : Successful Test of Remote Probing," *Science*, **169**, pp. 1256-1258, 1969.

Zenone, R. J., "Advanced Microwave Sounding Unit-A," *NOAA Technical Reports NESDIS 35*, pp. 167 - 173, 1987.